Network Approximation for Transport Properties of High Contrast Materials

Liliana Borcea*, and George C. Papanicolaou†

November 4, 1996

Abstract

We show that the effective complex impedance of materials with conductivity and dielectric permittivity that have high contrast can be calculated approximately by solving a suitable resistor-capacitor network. We use extensively variational principles for the analysis and we assess the accuracy of the network approximation by numerical computations.

Contents

*Scientific Computing and Computational Mathematics, Stanford University, Stanford, CA 94305, email: borcea@sccm.stanford.edu

†Dept of Mathematics, Stanford University, Stanford, CA 94305, email: papanico@georgep.stanford.edu

1 Introduction

The overall electric or other transport properties of materials whose conductivity, dielectric permittivity, etc undergo large variations over short distances are difficult to calculate both analytically and numerically. In this paper we show that in many situations the overall or effective transport properties can be approximated by those of a resistor-capacitor network.

High contrast electromagnetic or hydraulic transport problems arise very frequently in geophysical applications and they are a serious obstacle in solving inverse problems [23], [1], [31]. This is because most imaging methods use some form of linearization of the unknown medium parameters about a uniform background (Born approximation), which cannot be done in high contrast situations. Understanding how high contrast in material properties affects overall transport behavior is an essential first step in improving imaging techniques [8].

One of the earliest high contrast problems that was solved analytically, by Keller [28], is the effective conductivity of a periodic array of perfectly conducting cylinders or spheres in a poorly conducting background. Keller's results were extended by Batchelor and O'Brien [4] to random arrangements of highly conducting grains in, or nearly in, contact with each other and immersed in a connected uniform matrix. Conductivity problems with checkerboard geometry were analyzed by Keller in [29]. Network or discrete circuit approximations have been used extensively in the past as a modeling tool for high contrast problems [3, 24, 33, 36, 37, 12] but the relationship to the underlying continuum problem is not made precise. Kozlov [34] first formulated and analyzed high contrast conductivity problems using variational methods when the approximating network consists of one resistor only. He formulated the calculation of the effective conductivity as a cell problem in homogenization of periodic structures [5, 27]. High contrast continuum problems are especially important in connection with imaging [8] where the material properties are not known and it is convenient to assume that the high contrast behavior arises in a simple, generic manner such as in a continuum.

Variational principles are used extensively to get bounds for the effective properties of heterogeneous and composite materials [35] (and the references cited there). However, these bounds deteriorate rapidly with high contrast because they do not contain accurate enough geometrical information about the approximating network. In the case of complex coefficients variational principles for the effective properties were obtained recently [11, 16] and they were used for bounds in [19]. They were

used for high contrast flow problems (large Peclet number effective diffusivity) and elsewhere in [16, 17, 18].

In this paper we consider general network approximations using again variational principles, including the ones for quasistatic transport problems where the equations have complex coefficients. We formulate the effective transport problem as in [34] both in the static (real coefficients) and quasistatic (complex coefficients) cases. We identify the approximating network of resistors in general, both in the static and in the quasistatic case, when there are many regions of flow concentration due to high contrast. We also present the results of extensive numerical simulations that assess the accuracy of the network approximation as a function of the contrast. We discuss our results and related issues in the Summary and Conclusions at the end of the paper.

In section 2 we formulate the calculation of the the effective conductivity and dielectric permittivity as a cell problem in the context of homogenization. We also introduce the variational principles which we use extensively in the analysis. In section 3 we review results for the effective conductivity of some two component periodic structures in order to motivate the results for the continuum problem, which are introduced in a heuristic, physical way in this section. In section 4 we give a detailed analysis of the network approximation based on the variational principles. In section 5 we present numerical computations that help establish the range of validity of the network approximation as a function of the contrast.

2 Quasistatic Electromagnetics and Associated Variational Principles

2.1 The Quasistatic Equations

We consider the system of Maxwell's equations in a domain Ω that contains no free charges or current sources, with electric and magnetic fields that have the form

$$\mathbf{E}(\mathbf{x},t) = \text{real}(\hat{\mathbf{E}}(\mathbf{x})e^{-i\omega t}), \tag{2.1}$$

$$\mathbf{H}(\mathbf{x},t) = \text{real}(\hat{\mathbf{H}}(\mathbf{x})e^{-i\omega t}), \tag{2.2}$$

where ω is the frequency of oscillation. The complex valued field amplitudes $\hat{\mathbf{E}}$ and $\hat{\mathbf{H}}$ satisfy the system

$$\begin{aligned} \nabla \times \hat{\mathbf{H}} &= \sigma\hat{\mathbf{E}} - i\omega\varepsilon\hat{\mathbf{E}} \\ \nabla \times \hat{\mathbf{E}} &= i\omega\mu\hat{\mathbf{H}} \\ \nabla \cdot (\varepsilon\hat{\mathbf{E}}) &= 0 \\ \nabla \cdot (\mu\hat{\mathbf{H}}) &= 0, \end{aligned} \tag{2.3}$$

where $\sigma(\mathbf{x})$ is the electric conductivity, $\varepsilon(\mathbf{x})$ is the dielectric permittivity and $\mu(\mathbf{x})$ is the magnetic permeability.

The system of equations (2.3) takes into account the conducting, dielectric and magnetic properties of the material. In conducting materials at low frequencies we have $\sigma \gg \omega\varepsilon$ and the dielectric term in (2.3) can be neglected. In this case only the magnetic and conducting properties are important. However, if the material is a poor conductor (e.g. glass, semiconductors, etc.) we cannot neglect the dielectric term. In fact, at low frequencies the magnetic properties of such materials are negligible. For example, if the size of the domain is 1 km and the relative dielectric permittivity and relative magnetic permeability are of order one, the magnetic properties of the material will be negligible for frequencies up to hundreds of kHz (see for example [7]).

Thus, the quasistatic approximation in dielectric media leads to the simplified system of equations which we consider throughout the rest of the paper

$$\begin{aligned} \hat{\mathbf{E}} &= (\rho + iC)\nabla \times \hat{\mathbf{H}} \\ \nabla \times \hat{\mathbf{E}} &= 0 \\ \nabla \cdot (\varepsilon \hat{\mathbf{E}}) &= 0 \\ \nabla \cdot (\mu \hat{\mathbf{H}}) &= 0. \end{aligned} \tag{2.4}$$

The first equation in (2.4) involves the complex impedance $\rho + iC$ which consists of a resistance (real part) and a capacitance or capacitive reactance (imaginary part), where

$$\rho(\mathbf{x}, \omega) = \frac{\sigma}{\sigma^2 + \omega^2\varepsilon^2}, \tag{2.5}$$

$$C(\mathbf{x}, \omega) = \frac{\omega\varepsilon}{\sigma^2 + \omega^2\varepsilon^2}. \tag{2.6}$$

By combining the first two equations in (2.4) we obtain

$$\nabla \times [(\rho + iC)\nabla \times \hat{\mathbf{H}}] = 0. \tag{2.7}$$

In two dimensions, the curl operator $\nabla\times$ is equivalent to the perpendicular gradient operator $\nabla^\perp = (-\partial_y, \partial_x)$ and since $\nabla \times \hat{\mathbf{H}}$ is a current density we use the notation $\nabla \times \hat{\mathbf{H}} = \mathbf{j}(\mathbf{x})$. Equation (2.7) becomes therefore

$$\begin{aligned} \nabla^\perp \cdot [(\rho + iC)\mathbf{j}] &= 0 \\ \nabla \cdot \mathbf{j} &= 0. \end{aligned} \tag{2.8}$$

Equations (2.7) or (2.8) can be used for composite materials with fine scale structure. In this context the microscopic fields can be averaged leading to an effective medium describing the large scale behavior of the material. In materials with periodic structure [5] the effective impedance of the composite can be obtained by solving (2.8) over a period cell when the average current over the cell is equal to a unit vector. Even though the method we describe in this paper is quite general, we will present it in the context of the periodic homogenization problem in two dimensions. Therefore we take

$$< \mathbf{j} >= \mathbf{e}_1, \tag{2.9}$$

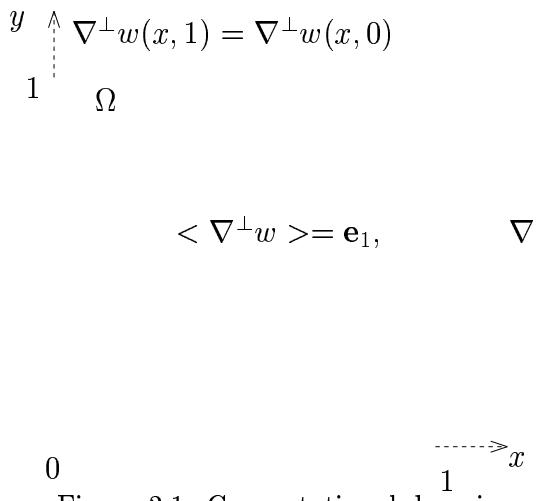

Figure 2.1: Computational domain

where $< \mathbf{j} >$ stands for the integral of $\mathbf{j}$ over the domain Ω, normalized by the area of Ω and $\mathbf{e}_j,\ j = 1, 2$ are unit vectors in the coordinate directions. According to (2.8) the field $\mathbf{j}$ is divergence free and so it can be expressed as the perpendicular gradient of a complex scalar function $w(\mathbf{x})$, $\mathbf{j}(\mathbf{x}) = \nabla^\perp w(\mathbf{x})$. The scalar function $w(\mathbf{x})$ is the component of the magnetic field perpendicular to the plane of the domain Ω (i.e. $\mathbf{H}(\mathbf{x}) = w(\mathbf{x})\mathbf{e}_3$). With this notation the system of equations (2.8) becomes

$$\begin{aligned} \nabla^\perp \cdot [(\rho + iC)\nabla^\perp w] &= 0 \\ < \nabla^\perp w > &= \mathbf{e}_1, \end{aligned} \tag{2.10}$$

where $\rho(\mathbf{x}), C(\mathbf{x})$, and $\nabla^\perp w(\mathbf{x})$ are periodic functions in the domain Ω as shown in Fig. 2.1. Equations (2.10) define the direct cell problem. Independently, by applying the divergence operator to the first equation in (2.4), and recalling that $\hat{\mathbf{E}}$ is curl free so that $\hat{\mathbf{E}} = -\nabla\phi$ is the gradient of the potential ϕ, we obtain the dual cell problem:

$$\begin{aligned} \nabla \cdot [\frac{1}{\rho + iC}\nabla\phi(\mathbf{x})] &= 0 \\ < \nabla\phi(\mathbf{x}) > &= \mathbf{e}_1. \end{aligned} \tag{2.11}$$

We will concentrate on the direct problem and rewrite the complex system of equations (2.10) as a system of real equations

$$\begin{aligned} \nabla^\perp \cdot [\rho\nabla^\perp u - C\nabla^\perp v] &= 0 \\ \nabla^\perp \cdot [C\nabla^\perp u + \rho\nabla^\perp v] &= 0 \\ < \nabla^\perp u > &= \mathbf{e}_1 \\ < \nabla^\perp v > &= \mathbf{0}, \end{aligned} \tag{2.12}$$

where we separated the function w into its real and imaginary parts $w(\mathbf{x}) = u(\mathbf{x}) + iv(\mathbf{x})$. It can be shown that if ρ and C are bounded functions and either one of them is strictly positive, the system of equations has a unique solution up to an additive constant. When ρ is strictly positive, it can easily be shown that (2.12) is elliptic and the Lax-Milgram lemma applies. However, we can rotate the system by 90 degrees in the complex plane (u, v) and notice that $C > 0$ is also a sufficient condition for the ellipticity of (2.12). The positivity of ρ has in fact a physical meaning as shown in [11]. The resistive part (ρ) of the microscopic impedance should always be greater than or equal to zero so that the dissipation energy averaged over a period of oscillations is positive

$$E_{dissip} = \frac{1}{2}\rho(\mid \text{real}(\hat{\mathbf{E}}) \mid^2 + \mid \text{imag}(\hat{\mathbf{E}}) \mid^2) \geq 0. \tag{2.13}$$

In our analysis, both ρ and C are greater than or equal to zero, with the constraint that they cannot vanish at the same location in Ω.

2.2 The Effective or Overall Impedance

The effective impedance associated with the direct problem is the average flux in the direction of the driving

$$\overline{Z} = < (\rho + iC)(\nabla^\perp u + i\nabla^\perp v) \cdot \mathbf{e}_1 > . \tag{2.14}$$

From equations (2.12) we conclude that the imaginary function v is periodic in Ω, whereas the real function u can be written as $u(\mathbf{x}) = -y + \psi(\mathbf{x})$, where $\psi(\mathbf{x})$ is a periodic function in Ω. The identity $\nabla^\perp \cdot (\phi\mathbf{a}) = \mathbf{a} \cdot \nabla^\perp\phi + \phi\nabla^\perp \cdot \mathbf{a}$, valid for any vector $\mathbf{a}$ and scalar function ϕ, and the periodicity of ρ, C, v, and ψ give

$$\begin{aligned} &< (\rho + iC)(\nabla^\perp u + i\nabla^\perp v) \cdot (\nabla^\perp \psi + i\nabla^\perp v) > \;\; = \\ &< \nabla^\perp \cdot [(\rho + iC)(\nabla^\perp u + i\nabla^\perp v)(\psi + iv)] > - \\ &\quad < (\psi + iv)\nabla^\perp \cdot [(\rho + iC)(\nabla^\perp u + i\nabla^\perp v)] > \;\; = \;\; 0. \end{aligned} \tag{2.15}$$

Consequently,

$$\overline{Z} = < (\rho + iC)(\nabla^\perp u + i\nabla^\perp v) \cdot (\nabla^\perp u + i\nabla^\perp v) > . \tag{2.16}$$

From (2.16) we obtain expressions for the effective resistance and capacitive reactance

$$\overline{R} = \text{real}(\overline{Z}) = < \rho \mid \nabla^\perp u \mid^2 > -2 < C\nabla^\perp u \cdot \nabla^\perp v > - < \rho \mid \nabla^\perp v \mid^2 >, \tag{2.17}$$

$$\overline{C} = \text{imag}(\overline{Z}) = < C \mid \nabla^\perp u \mid^2 > +2 < \rho\nabla^\perp u \cdot \nabla^\perp v > - < C \mid \nabla^\perp v \mid^2 > . \tag{2.18}$$

2.3 The Variational Principles

The real and imaginary part of the effective impedance $\overline{Z}$ can also be obtained by using the following saddle-point variational principles

$$\begin{aligned} \overline{R} = \min_{<\nabla^\perp u> = \mathbf{e}_1} \max_{<\nabla^\perp v> = \mathbf{0}} (&< \rho \mid \nabla^\perp u \mid^2 > -2 < C\nabla^\perp u \cdot \nabla^\perp v > - \\ &< \rho \mid \nabla^\perp v \mid^2 >), \end{aligned} \tag{2.19}$$

$$\overline{C} = \min_{<\nabla^\perp u>=\mathbf{e}_1} \max_{<\nabla^\perp v>=\mathbf{0}} (< C \mid \nabla^\perp u \mid^2 > +2 < \rho \nabla^\perp u \cdot \nabla^\perp v > - < C \mid \nabla^\perp v \mid^2 >) \tag{2.20}$$

This is because the Euler equations for (2.19) and (2.20) coincide with equations (2.12). Variational principles of this and related forms were introduced by Cherkaev and Gibiansky [11] and by Fannjiang and Papanicolaou [16]. Besides these variational principles of saddle point type, this problem also has variational principles of Dirichlet type (min min or max max). In general variational principles of Dirichlet type are preferred to saddle point ones in obtaining bounds on the effective parameters and especially in numerical computations. However, the Euler equations associated with them are difficult to use because they are in terms of both current and potential gradients and the coefficients are nonlinear functions of of ρ and C.

We chose to work with the saddle point variational principles (2.19) and (2.20) because they are quite suitable to our particular problem of estimating the effective impedance of high contrast media. This is because an asymptotic analysis performed on the simpler system of Euler equations (2.12) can provide a good guess of the trial fields $\mathbf{j}_R$ and $\mathbf{j}_I$. For example, in order to get an upper bound on the effective resistance $\overline{R}$ from (2.19) we can use such a guess for the real part of the current. Then we are left with a single maximization problem. In general this problem will be difficult to solve but in our case the maximization is equivalent to the minimization occurring in the computation of the effective real conductivity of isotropic media for static fields. The later is a problem we can solve asymptotically (see §4) and therefore we can obtain an upper bound on $\overline{R}$. A similar strategy is used in obtaining a lower bound on $\overline{R}$. This procedure is used in the proofs we present and works well for high contrast media.

2.4 The High Contrast Model

Our aim in this paper is to study the behavior of the effective resistance and capacitance when the microscopic resistance and capacitance have logarithmic high contrast behavior. We assume that the high contrast arises in a simple, generic manner as a continuum and propose the model

$$\begin{aligned} \rho(\mathbf{x}) &= \rho_0 e^{-\frac{S(\mathbf{x})}{\epsilon^2}}, \\ C(\mathbf{x}) &= C_0 e^{-\frac{P(\mathbf{x})}{\epsilon^2}} \end{aligned} \tag{2.21}$$

where $S(\mathbf{x})$ and $P(\mathbf{x})$ are smooth, periodic functions defined on Ω, ϵ is a small parameter and ρ_0, C_0 are constants which can be viewed as the microscopic resistance and capacitive reactance of a homogeneous reference medium. Model conductivities of form (2.21) were used by Kozlov [34] and Golden and Kozlov [21] for continuum percolation models of media with large variations that are exactly solvable in the asymptotic limit of infinitely high contrast. Model conductivities of the form (2.21) were also used in imaging high contrast conductivities from d.c. electric boundary

measurements [8]. The high contrast asymptotic analysis is carried out for random resistance and capacitance in the form (2.21) in [9]. Connections with percolation theory are used in [21, 20], as well as in [34, 6, 18].

In the following sections we analyze the behavior of the effective impedance and the current flow in Ω when ρ and C have the form (2.21) and ϵ is small. We can easily see from (2.21) that when the contrast is high ($\epsilon \ll 1$), the resistance will dominate the capacitance when its scaled logarithm $S(\mathbf{x})$ is less than $P(\mathbf{x})$. In fact, ρ and C are comparable in magnitude only when $S(\mathbf{x})$ equals $P(\mathbf{x})$. However, in general one does not expect $S(\mathbf{x})$ to be equal to $P(\mathbf{x})$ over large regions in the domain so we model the medium by alternating regions of dominant resistance and capacitance. Because both ρ and C are assumed to be general continuous functions, the regions are separated by interfaces along which ρ is equal to C.

3 Asymptotic Analysis of High Contrast Problems

To understand better the behavior of the effective impedance in high-contrast composites we first analyze some simpler problems. This will also explain the physical meaning of the results.

3.1 Review of Effective Conductivity Calculations for Some Special Two Component Composites

In the static case $\omega = 0$ we have from (2.5) and (2.6) that $\rho(\mathbf{x}) = \frac{1}{\sigma}, C = 0$ and the medium is purely resistive. The direct cell problem (2.10) reduces then to

$$\begin{aligned} \nabla^{\perp} \cdot (\rho \mathbf{j}) &= 0 \\ \nabla \cdot \mathbf{j} &= 0 \\ < \mathbf{j} > &= \mathbf{e}_1. \end{aligned} \tag{3.1}$$

The current flowing in the domain Ω is real and the effective resistance is

$$\overline{R} =< \rho \mathbf{j} \cdot \mathbf{j} > . \tag{3.2}$$

The dual of this problem for the electric potential ϕ has from (2.11) the form

$$\begin{aligned} \nabla \cdot (\sigma \nabla \phi) = 0 \\ < \nabla \phi >= \mathbf{e}_1, \end{aligned} \tag{3.3}$$

with the effective conductivity given by

$$\overline{\sigma} =< \sigma \nabla \phi \cdot \nabla \phi > . \tag{3.4}$$

It is well known (see for example [27]) that $\overline{\sigma} = \frac{1}{\overline{R}}$.

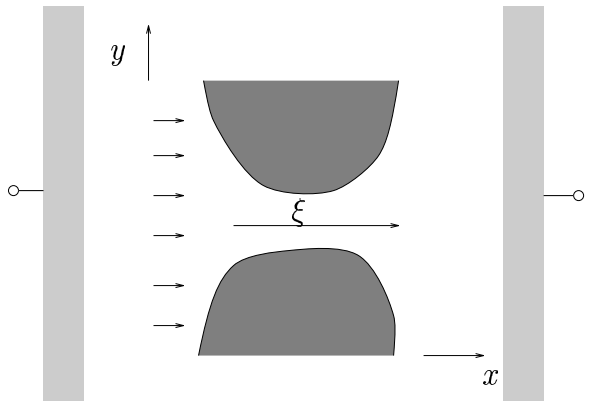

Figure 3.1: Flow channeling in a high contrast, two component medium

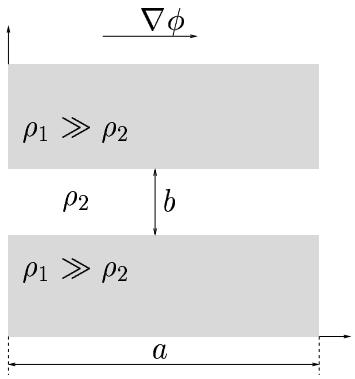

Figure 3.2: Current flow in a channel

Before attempting to solve this problem in the continuous high contrast case we study it first for some discontinuous two component composites. We consider problems like the one shown in Fig. 3.1 where the resistance of the material in the period cell can take only two values ρ_1 (for the black region) and ρ_2 (for the white region). Since we are interested in high contrast we assume that $\rho_1 \gg \rho_2$. Between the left and right boundaries of the domain we apply a potential difference $\nabla\phi$, in the x direction, and study the flow of electric current through the cell. We expect that the current will tend to pass through regions of small resistance. Since we assumed the resistance in the black region (ρ_1) to be very high, the only way the current can pass through the barrier shown in Fig. 3.1 is by concentrating in the channel near the point ξ. In the rest of the domain the current will be diffuse in the white region and will be much smaller than its value near the point ξ. It will be negligible in the black region. The effective resistance of this composite is determined by the resistance (R) of the channel. We expect R to decrease if the width of the channel increases or the

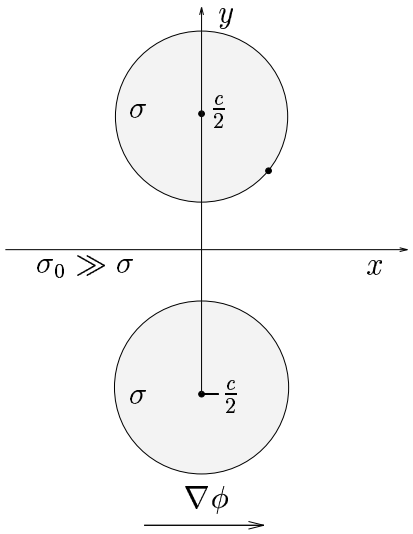

Figure 3.3: Insulating cylinders in a conducting background

radius of curvature of the isolating regions decreases. If the width of the channel is b and the radius of curvature of the isolating regions is a we therefore expect a result of the form $R \approx \rho_2 f(\frac{a}{b})$, where f is a monotone increasing function. At the point ξ we can take the curvature in the y direction to be $k_1 = \frac{1}{b}$ and the curvature in the x direction to be $k_2 = \frac{1}{a}$ and obtain

$$\overline{R} \approx \rho_2 f(\frac{a}{b}) = \rho_2 f(\frac{k_1}{k_2}). \tag{3.5}$$

We do not know the exact form of the function $f(\cdot)$ but we expect it to depend on the geometry of the problem. To illustrate (3.5) we consider some simple geometries.

We start with the case shown in figure 3.2. We have a conducting channel of resistance ρ_2 embedded in an isolating background ($\rho_1 \gg \rho_2$). When we apply a unit potential difference $\nabla\phi$ between the ends of the channel all the current will flow through it. The electric current density is $\mathbf{j} = \rho_2^{-1}\mathbf{e}_1$ and its average over the domain is $< \mathbf{j} >= \rho_2^{-1} b\mathbf{e}_1$. The effective resistance is computed from (3.2)

$$\overline{R} \approx \frac{1}{(b\rho_2^{-1})^2} \int_{-b/2}^{b/2} \int_{-\frac{a}{2}}^{\frac{a}{2}} \rho_2(\rho_2^{-1})^2 dxdy = \rho_2 \frac{a}{b}. \tag{3.6}$$

This result agrees with the heuristic form (3.5) if we take the function $f(x) = x$.

The next problem was analyzed by Keller [28]. We consider a periodic array of nonconducting cylinders ($\sigma = 0$) embedded in a conducting uniform background σ_0 (see Fig. 3.3). The cylinders have radius a and their axes are at distance c apart. We assume that an electric field is applied in the x direction and compute the effective resistance of the composite. When the cylinders touch each other it is clear that the

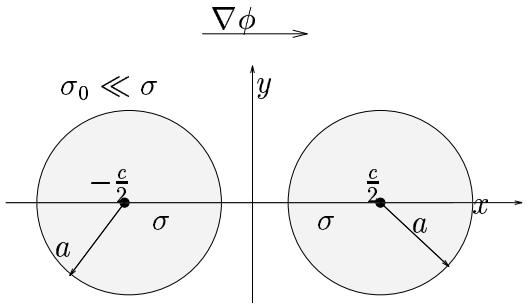

Figure 3.4: Conducting cylinders in an insulating background

effective conductivity is zero so we are interested in the case of a narrow channel (i.e., $b = c - 2a$ small). The electric current concentrates in the channel and the effective resistance is given by

$$\overline{R} \approx \sigma_0^{-1} \pi \sqrt{\frac{a}{b}}, \tag{3.7}$$

where $b = c - 2a$ is the width of the channel. This result agrees with (3.5) with $f(x) = \pi\sqrt{x}$ which is different from the previous case.

Another configuration, also analyzed by Keller [28], is shown in Fig. 3.4. We have a periodic array of perfectly conducting cylinders ($\sigma \to \infty$) embedded in a uniform insulating background ($\sigma_0 \ll \sigma$). The cylinders have their axes a distance c apart and their radii are equal to a. When we apply an electric field in the x direction we have current flowing through the gap between the cylinders. When the cylinders touch each other the effective conductivity is infinite so we are interested in narrow gaps. The effective resistance of this composite is

$$\overline{R} \approx \sigma_0^{-1} \pi^{-1} \sqrt{\frac{c - 2a}{a}} = \sigma_0^{-1} \pi^{-1} \sqrt{\frac{b}{a}}, \tag{3.8}$$

which is the reciprocal of (3.7).

These results can be easily extended to cylindrical inclusions of different radii. If the conducting cylinders in figure 3.4 have radii a_1 and a_2, with c the intercenter distance and $b = c - (a_1 + a_2)$ the gap, then the effective resistance is given by

$$\overline{R} \approx \sigma_0^{-1} \pi^{-1} \sqrt{\frac{(a_1 + a_2) b}{2 a_1 a_2}}, \tag{3.9}$$

which reduces to (3.8) when the radii are equal $a_1 = a_2 = a$.

All the cases considered so far confirm the expression (3.5), with different forms for the function $f(\cdot)$, the common feature being current channeling in regions of high contrast.

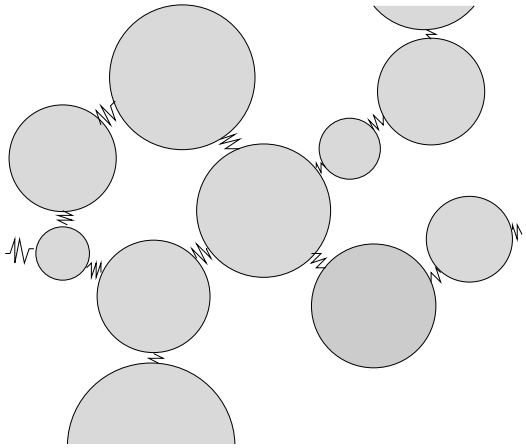

Figure 3.5: The effective resistor network for high-conductivity cylindrical inclusions.

If there are several conducting cylinders in the region (Fig. 3.5) then the overall conductivity can be calculated by solving the resistor network, shown in Fig. 3.5, in which each resistance is given by a formula like (3.9).

We consider now another two component configuration that is different from the previous ones because there are no channels. It is the checkerboard geometry shown in Fig. 3.6 and analyzed by Keller in [29]. The rectangles have conductivities σ_1 and σ_2 with $\sigma_2 \gg \sigma_1$. The effective conductivity tensor $\overline{\sigma}$ has its principal axes in the x and y directions and is diagonal. Because $\sigma_2 \gg \sigma_1$, the current flows from one conducting region to another across the corner so the effective conductivity of the composite is controlled by the conductivity of the corner. In fact, the effective resistance is $\overline{R} \approx \frac{1}{\sigma_c} h_2/h_1$, where the conductivity of the corner is $\sigma_c = \sqrt{\sigma_1 \sigma_2}$. This result is different from (3.5). While the factor h_2/h_1 suggests a geometry dependent function $f(x) = x$, the absence of a channel leads to an effective resistance depending on the geometric average of the component resistances rather than on the resistance of only one component.

Similar asymptotic techniques can be used in the computation of effective conductivity of high contrast discontinuous materials in three dimensions. Keller [28] studied such a problem for a dense cubic periodic array of perfectly conducting identical spheres immersed in a material of small uniform conductivity σ_0. For a dense packing, Keller shows that most of the current flows across narrow gaps separating adjacent spheres and that the leading term in the asymptotic approximation of the effective conductivity is

$$\overline{\sigma} \approx \frac{\sigma_0 \pi}{2} log(\frac{a}{h}), \tag{3.10}$$

where a is the radius of the spheres and h is the width of the gap. The asymptotic approximation (3.10) agrees with the heuristic result (3.5) stated in the two-dimensional case and shows that when the spheres touch each other the effective conductivity has

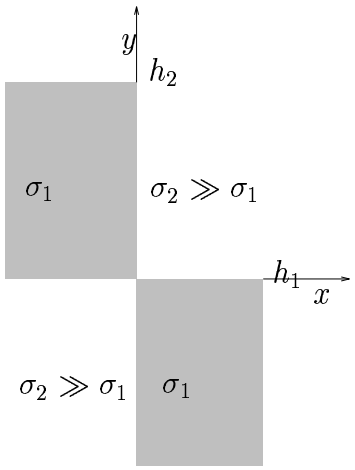

Figure 3.6: Rectangular checkerboard

a logarithmic singularity.

We consider next continuous media with logarithmic high contrast properties.

3.2 Local Analysis of Static Transport Properties of a High Contrast Continuum

We restrict attention first to a purely resistive problem (equations (3.1), (3.2)) for a continuous medium with the microscopic resistance $\rho(\mathbf{x}) = \rho_0 e^{-\frac{S(\mathbf{x})}{\epsilon^2}}$. The geometry of the composite is sketched in figure 3.7. The microscopic resistance $\rho(\mathbf{x})$ has two minima at $\mathbf{x}_{m1}$ and $\mathbf{x}_{m2}$, two maxima at $\mathbf{x}_{M1}$ and $\mathbf{x}_{M2}$, and a saddle point $\mathbf{x}_s$. At this point the function $\rho(\mathbf{x})$ is maximum in the x direction and minimum in the y direction. In a small neighborhood of $\mathbf{x}_s$ the function S has the approximate expression

$$S(\mathbf{x}) \approx S(\mathbf{x}_s) + \frac{k^-(x - x_s)^2}{2} - \frac{k^+(y - y_s)^2}{2}. \tag{3.11}$$

The geometry we consider here is the continuous equivalent of the discrete case we presented before and, therefore, we expect the following flow behavior.

The effective resistance is given by $\overline{R} \approx \rho(\mathbf{x}_s)\sqrt{\frac{k^+}{k^-}}$ *with the flow concentrated in the driving direction around the saddle point* $\mathbf{x}_s$.

We give a heuristic derivation of this result motivated by the previous examples and return in §4 to give a proof based on variational principles. Just like the previous cases the current will be small in regions with high resistance and in particular in the vicinity of the maxima $\mathbf{x}_{M1}$ and $\mathbf{x}_{M2}$. Around the minima $\mathbf{x}_{m1}$ and $\mathbf{x}_{m2}$, the

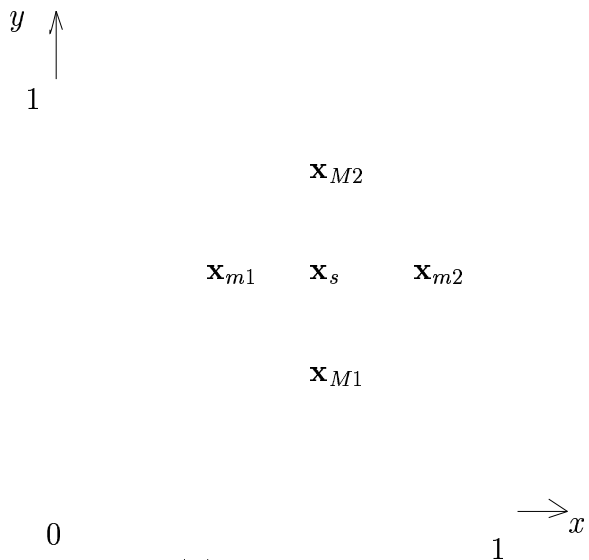

Figure 3.7: Resistance $\rho(\mathbf{x})$ with a single saddle point in the domain

bowl shaped resistance function $\rho(\mathbf{x})$ will cause the flow to stall. The only way for the current to pass through the highly resistive region created by the two maxima of $\rho(\mathbf{x})$ is by concentrating in a small neighborhood of the saddle point $\mathbf{x}_s$. The small neighborhood of the saddle-point acts like a bottleneck for the current flow, so it is sufficient to solve the cell problem (3.1) in the vicinity of $\mathbf{x}_s$ and to look for a current in the x direction. The current is given by $\mathbf{j} = \nabla^{\perp} u$, where u can be viewed as the magnetic field in the direction perpendicular to Ω. In order for the current to be in the x direction, u must be a function of y only. In a small neighborhood of $\mathbf{x}_s$, where $S(\mathbf{x})$ has the expression (3.11), the direct cell problem (3.1) simplifies to

$$\frac{d}{dy}[exp(\frac{k^+(y-y_s)^2}{2\epsilon^2})\frac{du}{dy}] = 0 \tag{3.12}$$

with the normalization condition

$$\int_{|y-y_s|\leq\delta}(-\frac{du}{dy})dy = 1 \tag{3.13}$$

for some $\delta > 0$ fixed.

Equation (3.12) gives $u'(y) = -D\cdot exp(-\frac{k^+(y-y_s)^2}{2\epsilon^2})$, where D is a constant obtained from (3.13): $D\sqrt{\frac{2\pi\epsilon^2}{k^+}} = 1$. The solution of the direct problem (3.1) is then

$$\mathbf{j} \approx \frac{1}{\sqrt{\frac{2\pi}{k^+}}\epsilon} exp(-\frac{k^+(y-y_s)^2}{2\epsilon^2})\mathbf{e}_1 \tag{3.14}$$

and by substituting it in (3.2) we obtain the effective resistance

$$\overline{R} \approx \rho(\mathbf{x}_s)\sqrt{\frac{2\pi}{k^-}}\epsilon\frac{1}{2\pi\epsilon^2}k^+\int_{y_s-\delta}^{y_s+\delta} exp(\frac{k^+(y-y_s)^2}{2\epsilon^2} - \frac{k^+(y-y_s)^2}{\epsilon^2})dy \approx$$

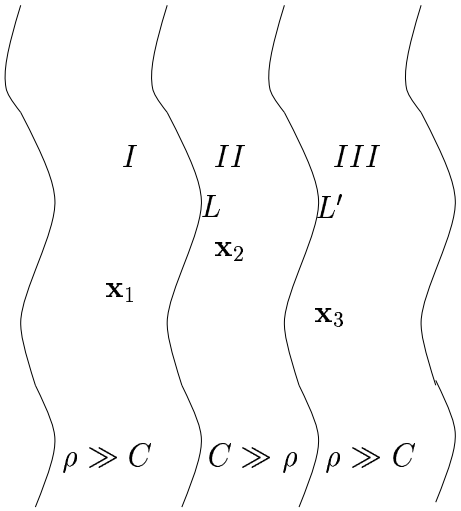

Figure 3.8: Medium layered across the driving direction

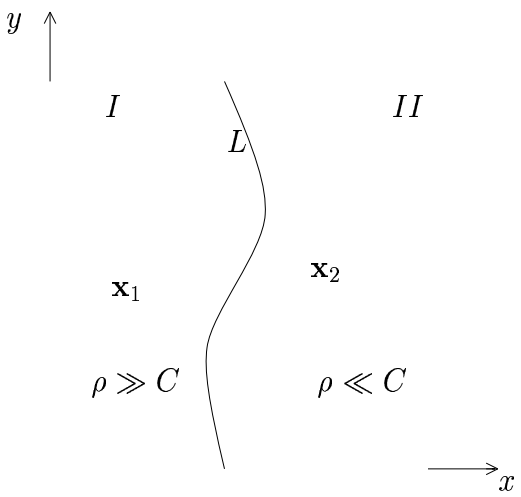

Figure 3.9: Enlarged view of the interface between two layers

$$\rho(\mathbf{x}_s)\sqrt{\frac{2\pi}{k^-}}\epsilon\frac{1}{2\pi\epsilon^2}k^+\sqrt{\frac{2\pi}{k^+}}\epsilon = \rho(\mathbf{x}_s)\sqrt{\frac{k^+}{k^-}}. \qquad (3.15)$$

Since the curvatures k^+, k^- have dimensions of $1/L^2$, this result for the effective resistance of the composite agrees with (3.5) with $f(x) = x$. In fact the result obtained here is more typical because the saddle points are just continuous versions of the channels, gaps or corners occurring in the discontinuous problems.

3.3 The Effective Quasistatic Impedance of a High Contrast Continuum

Case A: Series Connection

We consider the direct problem (2.12) with the coefficients ρ and C given by (2.21), defined over a region with the geometry shown in Fig. 3.8. The domain is divided in three regions by curves L and L'. In regions I and III the resistance dominates and has the saddle points $\mathbf{x}_1 \in$ region I and $\mathbf{x}_3 \in$ region III oriented in the x direction. In region II the capacitance is dominant and has a saddle point $\mathbf{x}_2$ oriented in the x direction. We choose this orientation of the saddles for simplicity. However, the results derived in this section apply to more general orientations, as well. The functions $\rho(\mathbf{x})$ and $C(\mathbf{x})$ are smooth and periodic and they equal each other along L and L'.

We apply a driving potential difference in the x direction and study the flow through the cell. From (2.12) we see that in each one of the regions of dominant capacitance or resistance the problem reduces to the one studied in §3.2. Thus, the current flow is concentrated at the saddle points of ρ and C and is oriented in the

driving direction x. The question that remains is how the three regions connect with each other. From Fig. 3.8 we see that it is sufficient to study the connection between regions I and II. The connection between regions II and III is similar. Thus, we concentrate attention to the domain shown in Fig. 3.9.

From the periodicity in y of the current and the lack of concentration of the vertical flow in both regions I and II we have

$$< \mathbf{j} >_I = < \mathbf{j} >_{II} = \mathbf{e}_1. \tag{3.16}$$

Thus, in region I, where the resistance is dominant, the problem reduces to

$$\begin{aligned} \nabla^{\perp}[\rho(\mathbf{j}_R + i\mathbf{j}_I)] &= 0 \\ \nabla \cdot \mathbf{j}_R &= \nabla \cdot \mathbf{j}_I = 0 \\ < \mathbf{j}_R > &= \mathbf{e}_1, \quad < \mathbf{j}_I >= \mathbf{0}, \end{aligned} \tag{3.17}$$

where $\mathbf{j}_R$, $\mathbf{j}_I$ are the real and imaginary current densities. It is easy to see that the imaginary current is zero, and that the problem reduces to the one studied in §3.2. A similar conclusion applies to region II where the capacitive reactance is dominant. Consequently, the flow behavior in regions I and II is exactly the one studied in section §3.2.

In the vicinity of the curve L the function $\rho(\mathbf{x})$ ($C(\mathbf{x})$) is continuously decreasing (increasing) with x. Because the flow is driven in the x direction, it must cross the curve L. The current will be diffuse in regions of this neighborhood where ρ and C are fairly flat, and it will concentrate close to the possible common minima of ρ and C along L. This current concentration is weaker than the one at saddle points because it occurs only along one direction (i.e. along L). There is no concentration in the direction perpendicular to the boundary interface and this leads to a lower order term in the effective impedance. In the asymptotic limit of infinitely high contrast the saddle points of ρ and C will dominate and the contribution of other features like the minima along L are negligible. This conclusion is supported by numerical experiments (see §5.2) and it is proved in §4 using variational principles. We should point out that the same kind of features can occur in the purely resistive problem and exactly as we concluded above they are negligible in the computation of the effective resistance for very high contrast. The validity of this is again given by variational principles (see §4.1). When the contrast is not very high, features other than the saddle points become important in the computation of $\overline{Z}$ as is seen in [10].

Thus, for computing the effective impedance we need only consider small neighborhoods of the saddle points of $\rho(\mathbf{x})$ and $C(\mathbf{x})$ in regions I, and II. Near these points we have

$$\rho(\mathbf{x}) \approx \rho(\mathbf{x}_1) exp(\frac{k_1^+(y-y_1)^2}{2\epsilon^2} - \frac{k_1^-(x-x_1)^2}{2\epsilon^2}), \quad | \mathbf{x} - \mathbf{x}_1 | < \delta \tag{3.18}$$

$$C(\mathbf{x}) \approx C(\mathbf{x}_2) exp(\frac{k_2^+(y-y_2)^2}{2\epsilon^2} - \frac{k_2^-(x-x_2)^2}{2\epsilon^2}), \quad | \mathbf{x} - \mathbf{x}_2 | < \delta \tag{3.19}$$

Figure 3.10: Equivalent Series Network

In these small regions we can solve our cell problem by separation of variables, exactly as in §3.2:

$$\begin{aligned}
\mathbf{j}_R &\approx \frac{1}{\sqrt{\frac{2\pi}{k_1^+}}\epsilon} exp(-\frac{k_1^+(y-y_1)^2}{2\epsilon^2})\mathbf{e}_1, \quad \mid \mathbf{x}-\mathbf{x}_1 \mid < \delta \\
\mathbf{j}_R &\approx \frac{1}{\sqrt{\frac{2\pi}{k_2^+}}\epsilon} exp(-\frac{k_2^+(y-y_2)^2}{2\epsilon^2})\mathbf{e}_1, \quad \mid \mathbf{x}-\mathbf{x}_2 \mid < \delta \qquad (3.20) \\
\mathbf{j}_I &\approx 0.
\end{aligned}$$

We use the expression (2.16) for the effective impedance and obtain

$$\begin{aligned}
\overline{Z} &\approx \rho(\mathbf{x}_1)\int_{y_1-\delta}^{y_1+\delta}\int_{x_1-\delta}^{x_1+\delta}\frac{1}{\frac{2\pi\epsilon^2}{k_1^+}} exp(-\frac{k_1^+(y-y_1)^2}{2\epsilon^2} - \frac{k_1^-(x-x_1)^2}{2\epsilon^2})dxdy + \\
&\quad iC(\mathbf{x}_2)\int_{y_2-\delta}^{y_2+\delta}\int_{x_2-\delta}^{x_2+\delta}\frac{1}{\frac{2\pi\epsilon^2}{k_2^+}} exp(-\frac{k_2^+(y-y_2)^2}{2\epsilon^2} - \frac{k_2^-(x-x_2)^2}{2\epsilon^2})dxdy \qquad (3.21) \\
&\approx \rho(\mathbf{x}_1)\sqrt{\frac{k_1^+}{k_1^-}} + iC(\mathbf{x}_2)\sqrt{\frac{k_2^+}{k_2^-}}.
\end{aligned}$$

This result, together with the observation that the current has the same normalized average over regions I or II as over the entire cell, tells us that our problem is asymptotically equivalent to the discrete series circuit shown in Fig. 3.10. We have only two network elements: one resistor $\overline{R} = \rho(\mathbf{x}_1)\sqrt{\frac{k_1^+}{k_1^-}}$ placed at $\mathbf{x}_1$, and a capacitor $\overline{C} = C(\mathbf{x}_2)\sqrt{\frac{k_2^+}{k_2^-}}$ placed at $\mathbf{x}_2$. The current passing through $\overline{R}$ is $< \mathbf{j}_R + i\mathbf{j}_I >_I = \mathbf{e}_1$, and the current passing through $\overline{C}$ is $< \mathbf{j}_R + i\mathbf{j}_I >_{II} = \mathbf{e}_1$.

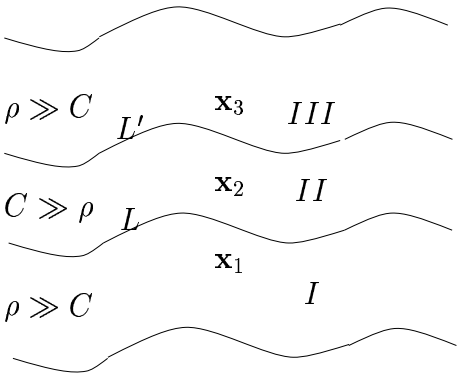

Figure 3.11: Medium layered along the driving direction

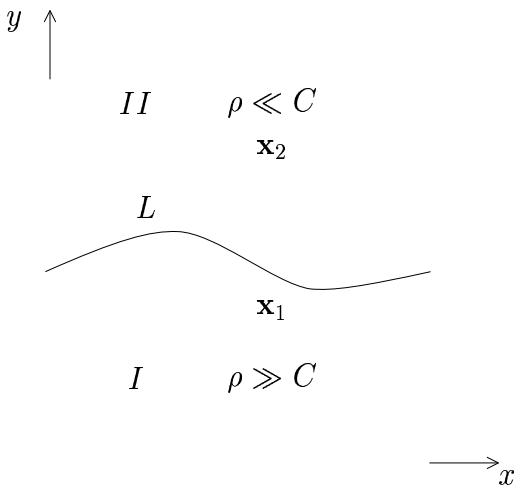

Figure 3.12: Enlarged view of the interface between two layers

Case B: Parallel Connection

We consider the direct problem (2.12) with the coefficients ρ and C given by (2.21), defined over a region with the geometry shown in Fig. 3.11. The domain is divided in three regions by curves L and L'. In regions I and III the resistance dominates and has the saddle points $\mathbf{x}_1 \in$ region I and $\mathbf{x}_3 \in$ region III oriented in the x direction. In region II the capacitance is dominant and has a saddle point $\mathbf{x}_2$ oriented in the x direction, as well. The functions $\rho(\mathbf{x})$ and $C(\mathbf{x})$ are smooth and periodic and they equal each other along L and L'.

We apply a driving potential difference in the x direction and study the flow through the cell. From (2.12) we obtain that

$$\begin{aligned} \nabla^{\perp} \cdot [\rho(\mathbf{j}_R + i\mathbf{j}_I)] &= 0 \text{ for } \mathbf{x} \in \text{region } I \text{ or } III \\ \nabla^{\perp} \cdot [C(\mathbf{j}_R + i\mathbf{j}_I)] &= 0 \text{ for } \mathbf{x} \in \text{region } II, \end{aligned} \tag{3.22}$$

where $\mathbf{j}_R$ and $\mathbf{j}_I$ are the real and imaginary current densities. The flow is driven in the x direction so we have $< \mathbf{j}_R + i\,\mathbf{j}_I >= K\mathbf{e}_1$, where K is a complex constant flux. We can rewrite the current densities as

$$\mathbf{j}_R = \text{real}(K)\mathbf{e}_1 + \nabla^{\perp} u,\ \mathbf{j}_I = \text{imag}(K)\mathbf{e}_1 + \nabla^{\perp} v,$$

where u and v can be viewed as the real and imaginary parts of the magnetic field. The functions $u(\mathbf{x})$ and $v(\mathbf{x})$ are periodic in the domain and satisfy the conditions

$$< \nabla^{\perp} u >=< \nabla^{\perp} v >= \mathbf{0}.$$

From the periodicity in x of both u and v it follows that in each region there is no

net flux in the y direction. For the flow in the x direction we have

$$\int_I \mathbf{j}\cdot\mathbf{e}_1 d\mathbf{x} + \int_{II} \mathbf{j}\cdot\mathbf{e}_1 d\mathbf{x} + \int_{III} \mathbf{j}\cdot\mathbf{e}_1 d\mathbf{x} = C\mathbf{e}_1 \tag{3.23}$$

which is equivalent to

$$\begin{aligned}
\int_i \mathbf{j}_R\cdot\mathbf{e}_1 d\mathbf{x} &= \alpha_i\mathbf{e}_1,\ i = I, II, \text{ or } III \\
\int_i \mathbf{j}_I\cdot\mathbf{e}_1 d\mathbf{x} &= \beta_i\mathbf{e}_1 \\
\sum_i \alpha_i &= \text{real}(K), \\
\sum_i \beta_i &= \text{imag}(K).
\end{aligned} \tag{3.24}$$

Equations (3.22) with the driving conditions (3.24) are very similar to the problem studied in §3.2 and give that the flow in each region of the domain is concentrated at the saddle points of ρ and C, respectively. The remaining question is how the regions connect with each other. We notice that the connection between regions I and II is similar to the connection between regions II and III. Thus, it is sufficient to study the flow in the domain shown in Fig. 3.12.

For simplicity we assume that the average flow over regions I and II is

$$\int_I \mathbf{j} d\mathbf{x} + \int_{II} \mathbf{j} d\mathbf{x} = \mathbf{e}_1.$$

A different driving condition with both real and imaginary net fluxes does not affect the expression of the effective impedance, it just modifies the fluxes of current in the channels (saddles). Consequently, we have

$$\begin{aligned}
\nabla^\perp\cdot[\rho(\mathbf{j}_R + i\mathbf{j}_I)] &= 0 \\
<\mathbf{j}_R> &= \alpha_1\mathbf{e}_1 \\
<\mathbf{j}_I> &= \beta_1\mathbf{e}_1 \\
\nabla\cdot\mathbf{j}_R &= \nabla\cdot\mathbf{j}_I = 0 \\
\mathbf{x} &\in \text{region } I,
\end{aligned} \tag{3.25}$$

$$\begin{aligned}
\nabla^\perp\cdot[iC(\mathbf{j}_R + i\mathbf{j}_I)] &= 0 \\
<\mathbf{j}_R> &= \alpha_2\mathbf{e}_1 \\
<\mathbf{j}_I> &= \beta_2\mathbf{e}_1 \\
\nabla\cdot\mathbf{j}_R &= \nabla\cdot\mathbf{j}_I = 0 \\
\mathbf{x} &\in \text{region } II.
\end{aligned} \tag{3.26}$$

In the vicinity of the curve L the function $\rho(\mathbf{x})$ ($C(\mathbf{x})$) is continuously decreasing (increasing) with y. In this region the current is diffuse and small where ρ and C

are fairly flat. If for example ρ and C have two maxima along L and a minimum in between, because we have no driving force in the y direction the current avoids the two maxima and is relatively small at the minimum as well. Consequently, the behavior of the flow for this problem is dictated by what happens in regions I, and II, for which we already know the result. This case is a little more complicated than case A because the current is divided between the two regions of our domain. Since the average current over the domain shown in Fig. 3.12 is $\mathbf{e}_1$, we must have

$$\begin{aligned} \alpha_1 + \alpha_2 &= 1 \\ \beta_1 + \beta_2 &= 0. \end{aligned} \tag{3.27}$$

We already know that in order to obtain the effective impedance of the regions I and II it is sufficient to look only in small neighborhoods of saddle points of ρ and C. In the vicinity of these points we have

$$\rho(\mathbf{x}) \approx \rho(\mathbf{x}_1) exp(\frac{k_1^+(y-y_1)^2}{2\epsilon^2} - \frac{k_1^-(x-x_1)^2}{2\epsilon^2}), \quad \mid \mathbf{x} - \mathbf{x}_1 \mid < \delta, \tag{3.28}$$

$$C(\mathbf{x}) \approx C(\mathbf{x}_2) exp(\frac{k_2^+(y-y_2)^2}{2\epsilon^2} - \frac{k_2^-(x-x_2)^2}{2\epsilon^2}), \quad \mid \mathbf{x} - \mathbf{x}_2 \mid < \delta \tag{3.29}$$

and by using separation of variables in (3.25) and (3.26) we obtain

$$\begin{aligned} \mathbf{j}_R + i\mathbf{j}_I &\approx \frac{\alpha_1}{\sqrt{\frac{2\pi}{k_1^+}\epsilon}} exp(-\frac{k_1^+(y-y_1)^2}{2\epsilon^2}) + i\frac{\beta_1}{\sqrt{\frac{2\pi}{k_1^+}\epsilon}} exp(-\frac{k_1^+(y-y_1)^2}{2\epsilon^2}), \quad \mid \mathbf{x} - \mathbf{x}_1 \mid < \delta \\ \mathbf{j}_R + i\mathbf{j}_I &\approx \frac{\alpha_2}{\sqrt{\frac{2\pi}{k_2^+}\epsilon}} exp(-\frac{k_2^+(y-y_2)^2}{2\epsilon^2}) + i\frac{\beta_2}{\sqrt{\frac{2\pi}{k_2^+}\epsilon}} exp(-\frac{k_2^+(y-y_2)^2}{2\epsilon^2}), \quad \mid \mathbf{x} - \mathbf{x}_2 \mid < \delta. \end{aligned} \tag{3.30}$$

We can use these results in the formula for the effective impedance (2.16) and, after performing straightforward computations, we obtain

$$\overline{Z} = [\overline{R}(\alpha_1^2 - \beta_1^2) - 2\overline{C}\alpha_2\beta_2] + i[\overline{C}(\alpha_2^2 - \beta_2^2) + 2\overline{R}\alpha_1\beta_1], \tag{3.31}$$

where $\overline{R} \approx \rho(\mathbf{x}_1)\sqrt{\frac{k_1^+}{k_1^-}}$ and $\overline{C} \approx C(\mathbf{x}_2)\sqrt{\frac{k_2^+}{k_2^-}}$. In order to determine the fluxes $\alpha_i, \beta_i, \quad i = 1, 2$ we look at the potential difference $\nabla\Phi(\mathbf{x})$ which is given by

$$\nabla\Phi(\mathbf{x}) = (\rho + iC)(\mathbf{j}_R + i\mathbf{j}_I). \tag{3.32}$$

We multiply equation (3.32) by $\mathbf{e}_1$ and average over the domain to obtain

$$< \nabla\Phi \cdot \mathbf{e}_1 >= \Delta U =< (\rho + iC)(\mathbf{j}_R + i\mathbf{j}_I) \cdot \mathbf{e}_1 >= \overline{Z}. \tag{3.33}$$

We can do the same thing for regions I and II. Because $\nabla\Phi$ is periodic over the cell and regions I and II have the same boundaries as the cell in the x direction, the

average potential difference for the entire cell equals the average potential difference over regions I and II. Consequently we have

$$\Delta U = \overline{Z} = \overline{R}(\alpha_1 + i\beta_1) = i\overline{C}(\alpha_2 + i\beta_2). \tag{3.34}$$

Relations (3.34) and (3.27) form a linear system of four equations and four unknowns with solution

$$\begin{aligned} \alpha_1 &= \frac{\overline{C}^2}{\overline{R}^2 + \overline{C}^2}, \\ \beta_1 &= \frac{\overline{RC}}{\overline{R}^2 + \overline{C}^2}, \\ \beta_2 &= -\frac{\overline{RC}}{\overline{R}^2 + \overline{C}^2}, \\ \alpha_2 &= \frac{\overline{R}^2}{\overline{R}^2 + \overline{C}^2}. \end{aligned} \tag{3.35}$$

Using (3.35) in (3.31) we obtain the following expression for the effective impedance

$$\overline{Z} = \frac{\overline{RC}^2}{\overline{R}^2 + \overline{C}^2} + i\frac{\overline{R}^2\overline{C}}{\overline{R}^2 + \overline{C}^2} = (\frac{1}{\overline{R}} + \frac{1}{i\overline{C}})^{-1}. \tag{3.36}$$

This result suggests that the continuous problem is asymptotically equivalent to the discrete network shown in Fig. 3.13, where a resistor $\overline{R}$ placed at $\mathbf{x}_1$ is connected in parallel with a capacitor $\overline{C}$ placed at $\mathbf{x}_2$. The current passing through $\overline{R}$ is $< \mathbf{j}_R + i\mathbf{j}_I >_I = \alpha_1\mathbf{e}_1 + i\beta_1\mathbf{e}_1$, and the current passing through $\overline{C}$ is $< \mathbf{j}_R + i\mathbf{j}_I >_{II} = \alpha_2\mathbf{e}_1 + i\beta_2\mathbf{e}_1$.

4 High Contrast Analysis Based on Variational Principles

In this section we prove that in the asymptotic limit of infinitely high contrast the computation of the effective impedance can be reduced to the solution of an equivalent network of resistors and capacitors. The effective impedance is given by

$$\overline{Z} = < (\rho + iC)\mathbf{j} \cdot \mathbf{j} > \tag{4.1}$$

where $\rho(\mathbf{x}) = \rho_0 e^{-\frac{S(\mathbf{x})}{\epsilon^2}}$, $C(\mathbf{x}) = C_0 e^{-\frac{P(\mathbf{x})}{\epsilon^2}}$ and $\mathbf{j}$ is the complex current density which satisfies

$$\begin{aligned} \nabla^\perp[(\rho + iC)\mathbf{j}] &= 0 \\ \nabla \cdot \mathbf{j} &= 0 \\ < \mathbf{j} > &= \mathbf{e}_1, \end{aligned} \tag{4.2}$$

over the periodic cell Ω. The effective impedance can also be obtained from variational principles of saddle point type (2.19) and (2.20). The proofs presented in this section assume a logarithmic high contrast of the coefficients ρ and C, as $\epsilon \to 0$.

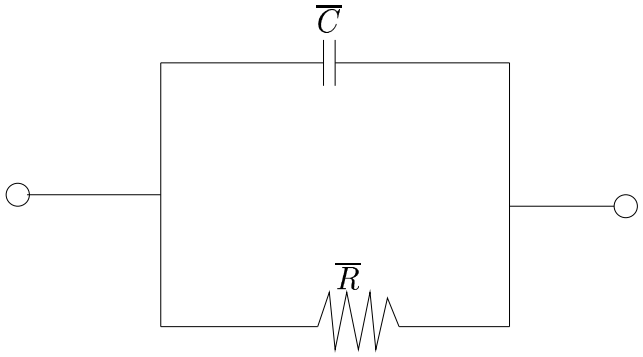

Figure 3.13: Equivalent Parallel Network

4.1 The High Contrast Approximation in the Static Case with One Channel

We return to the problem considered in §3.2 in the static, purely resistive circuit, with $\rho(\mathbf{x}) = \rho_0 e^{-\frac{S(\mathbf{x})}{\epsilon^2}}$. The function $S(\mathbf{x})$ is smooth and periodic. The geometry of the composite is sketched in figure 3.7. The resistance $\rho(\mathbf{x})$ has two minima at $\mathbf{x}_{m1}$ and $\mathbf{x}_{m2}$, two maxima at $\mathbf{x}_{M1}$ and $\mathbf{x}_{M2}$, and a saddle point $\mathbf{x}_s$. Near the saddle point we have

$$S(\mathbf{x}) \approx S(\mathbf{x}_s) + \frac{k^-(x - x_s)^2}{2} - \frac{k^+(y - y_s)^2}{2}. \tag{4.3}$$

Under these assumptions we state the following theorem:

Theorem 1. The effective resistance is given by

$$\overline{R} \approx \rho(\mathbf{x}_s)\sqrt{\frac{k^+}{k^-}}, \tag{4.4}$$

with the flow in the driving direction and concentrated around the saddle point $\mathbf{x}_s$.

The proof of this theorem is based on the variational principles and it was first given by Kozlov [34]. We define the direct cell problem

$$\begin{aligned} \nabla^{\perp} \cdot (\rho \mathbf{j}) &= 0 \\ < \mathbf{j} > &= \mathbf{e}_1 \\ \nabla \cdot \mathbf{j} &= 0 \end{aligned} \tag{4.5}$$

with the associated effective resistance

$$\overline{R} =< \rho \mathbf{j} \cdot \mathbf{j} >, \tag{4.6}$$

and the dual cell problem

$$\begin{aligned} \nabla \cdot (\frac{1}{\rho}\nabla\phi) &= 0 \\ <\nabla\phi> &= \mathbf{e}_1 \end{aligned} \tag{4.7}$$

with the effective conductivity

$$\overline{\sigma} =< \frac{1}{\rho}\nabla\phi \cdot \nabla\phi > . \tag{4.8}$$

The effective parameters $\overline{R}$, and $\overline{\sigma}$ can also be obtained from the Dirichlet-type variational principles

$$\overline{R} = \min_{<\nabla^\perp u>=\mathbf{e}_1} < \rho\nabla^\perp u \cdot \nabla^\perp u >, \tag{4.9}$$

$$\overline{\sigma} = \min_{<\nabla\phi>=\mathbf{e}_1} < \frac{1}{\rho}\nabla\phi \cdot \nabla\phi > \tag{4.10}$$

since the Euler equations associated with them are exactly (4.5), and (4.7). Note that in (4.9) we replaced the current density by $\mathbf{j} = \nabla^\perp u$, where u is the magnitude of the magnetic field which is perpendicular to the plane of Ω. We begin with a lemma which is proved in [27], pp. 199-200.

Lemma 1. The effective parameters $\overline{R}$ and $\overline{\sigma}$ satisfy the relation $\overline{R} = \overline{\sigma}^{-1}$.

In order to prove Theorem 1, we will obtain an upper bound for $\overline{R}$ from (4.9) which we will match with a lower bound for $\overline{R}$ obtained from the dual variational principle (4.10).

If we select from the eligible fields $\nabla^\perp u$ in (4.9), those which are nonzero only in a neighborhood of $\mathbf{x}_s$, we obtain the inequality

$$\overline{R} \lesssim \min_{<\nabla^\perp u>_\delta=\mathbf{e}_1} \int_{|\mathbf{x}-\mathbf{x}_s|\le\delta} \rho \mid \nabla^\perp u \mid^2 d\mathbf{x}, \tag{4.11}$$

where $< \nabla^\perp u >_\delta$ is the average of $\nabla^\perp u$ in the δ - neighborhood of the saddle point. From all the possible fields $\nabla^\perp u$ in (4.11) we choose those which have the component in the direction $\mathbf{e}_2$ equal to zero, so that $u = u(y)$ only, and therefore we obtain

$$\overline{R} \lesssim \int_{x_s-\delta}^{x_s+\delta} \rho(\mathbf{x}_s) exp(-\frac{k^-(x-x_s)^2}{2\epsilon^2})dx \int_{y_s-\delta}^{y_s+\delta} exp(\frac{k^+(y-y_s)^2}{2\epsilon^2})(\frac{du}{dy})^2 dy, \tag{4.12}$$

where $\int_{y_s-\delta}^{y_s+\delta}(-\frac{du}{dy})dy = 1$. We point out that the inequalities above are only asymptotic and depend on the parameter δ which is fixed as $\epsilon \to 0$. More precisely, $\overline{R} \lesssim F^{\epsilon,\delta}$ means $\overline{R} \le F^{\epsilon,\delta}(1 + o(1))$ with the small order one term tending to zero as $\epsilon \to 0$ with $\delta > 0$ fixed. After doing the x integration, (4.12) becomes

$$\overline{R} \lesssim \rho(\mathbf{x}_s)\sqrt{\frac{2\pi}{k^-}}\epsilon \min_u \int_{y_s-\delta}^{y_s+\delta} exp(\frac{k^+(y-y_s)^2}{2\epsilon^2})(\frac{du}{dy})^2 dy. \tag{4.13}$$

We choose u in (4.13) to minimize the right side. Then u satisfies the Euler equation

$$\begin{aligned} \frac{d}{dy}[exp(\frac{k^+(y-y_s)^2}{2\epsilon^2})\frac{du}{dy}] &= 0 \\ \int_{y_s-\delta}^{y_s+\delta}(-\frac{du}{dy})dy &= 1. \end{aligned} \tag{4.14}$$

Equations (4.14) are exactly the same as (3.12) and u is given by (3.14), which substituted in (4.13) gives the upper bound

$$\overline{R} \lesssim \rho(\mathbf{x}_s)\sqrt{\frac{2\pi}{k^-}}\epsilon\frac{1}{2\pi\epsilon^2}k^+\int_{y_s-\delta}^{y_s+\delta} exp(\frac{k^+(y-y_s)^2}{2\epsilon^2} - \frac{k^+(y-y_s)^2}{\epsilon^2})dy = \rho(\mathbf{x}_s)\sqrt{\frac{2\pi}{k^-}}\epsilon\frac{1}{2\pi\epsilon^2}k^+\sqrt{\frac{2\pi}{k^+}}\epsilon = \rho(\mathbf{x}_s)\sqrt{\frac{k^+}{k^-}}, \tag{4.15}$$

This bound is gotten under the hypothesis that the current $\nabla^\perp u$ is concentrated around $\mathbf{x}_s$, and flows in the driving direction. To obtain a lower bound for $\overline{R}$ we use the dual formulation with the variational principle (4.10) and Lemma 1. In (4.10) we select fields $\nabla\phi$ which are concentrated around $\mathbf{x}_s$ and have nonzero components only in the $\mathbf{e}_1$ direction. The minimum over such fields can only give a larger value of the functional in (4.10) and we obtain

$$\overline{\sigma} \lesssim \min_{\phi}\int_{x_s-\delta}^{x_s+\delta}\rho^{-1}(\mathbf{x}_s)exp(\frac{k^-(x-x_s)^2}{2\epsilon^2})(\frac{d\phi}{dx})^2dx\int_{y_s-\delta}^{y_s+\delta}exp(-\frac{k^+(y-y_s)^2}{2\epsilon^2})dy, \tag{4.16}$$

where $\int_{x_s-\delta}^{x_s+\delta}(\frac{d\phi}{dx})dx = 1$. The computation for the minimum in (4.16) is exactly the same as the one for the direct problem. By solving the Euler equation associated with (4.16) we obtain

$$\frac{d\phi}{dx} = \frac{1}{\sqrt{\frac{2\pi}{k^-}\epsilon}}exp(-\frac{k^-(x-x_s)^2}{2\epsilon^2}) \tag{4.17}$$

and hence

$$\overline{\sigma} \lesssim \rho^{-1}(\mathbf{x}_s)\sqrt{\frac{2\pi}{k^+}}\epsilon\frac{1}{\frac{2\pi}{k^-}\epsilon^2}\int_{x_s-\delta}^{x_s+\delta}exp(\frac{k^-(x-x_s)^2}{2\epsilon^2} - \frac{k^-(x-x_s)^2}{\epsilon^2})dx = \rho^{-1}(\mathbf{x}_s)\sqrt{\frac{2\pi}{k^+}}\epsilon\frac{1}{\frac{2\pi}{k^-}\epsilon^2}\sqrt{\frac{2\pi}{k^-}}\epsilon. \tag{4.18}$$

Using Lemma 1 and (4.18) we see that $\overline{R}$ satisfies

$$\overline{\sigma} = \overline{R}^{-1} \lesssim \rho^{-1}(\mathbf{x}_s)\sqrt{\frac{k^-}{k^+}}. \tag{4.19}$$

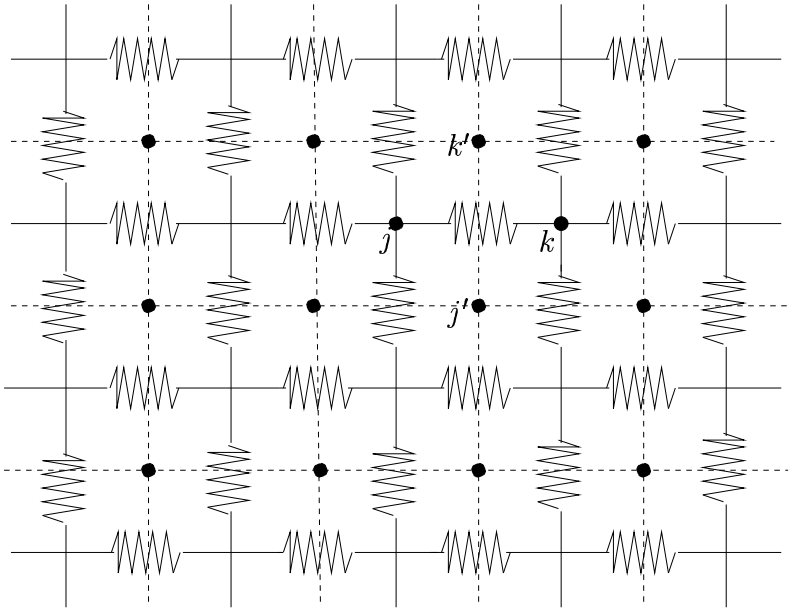

Figure 4.1: Periodic resistor network

Combining (4.15), and (4.19) we get the asymptotic behavior of the effective resistance

$$\overline{R} \approx \rho(\mathbf{x}_s)\sqrt{\frac{k^+}{k^-}}. \tag{4.20}$$

Since we used a current $\nabla^\perp u$ in the $\mathbf{e}_1$ direction and concentrated around $\mathbf{x}_s$ to get (4.20), Theorem 1 is proved.

4.2 High Contrast Approximation in the Static Case with Many Channels

We shall now describe how to analyze (3.1)-(3.2) and (3.3)-(3.4) when $\rho(\mathbf{x})$ has several, say $M \geq 2$, saddle points in Ω.

With each saddle point we associate an effective resistance $\overline{R}_j,\ j = 1, 2, \ldots, M$ given by the right side of (4.4). This comes from the local analysis around a saddle point that was just carried out in Theorem 1. To find the currents flowing through the saddle points we must specify how the effective saddle resistances are connected to each other. We do this by identifying the network associated with the resistance function $\rho(\mathbf{x})$ as follows.

With each minimum of the resistance $\rho(\mathbf{x})$ we associate a node of a network on the torus T^2 (which is the region Ω). The nodes are connected to adjacent nodes if there is a path between two nodes that goes over a single saddle. This path is a branch or a bond that connects two nodes. To avoid complicated terminology and

notation we will assume that the network that is associated with the resistance is a rectangular lattice network as in the figure 4.1. Recall that the network is periodic.

Let the index $j \in N$ denote the set of nodes and I_{jk} be the current from node j to node k that is a neighbor of j, $k \in N_j$. Then $I_{jk} = -I_{kj}$ and

$$\sum_{k \in N_j} I_{jk} = 0, \ j \in N \tag{4.21}$$

which is the discrete analog of $\nabla \cdot \mathbf{j} = 0$, Kirchoff's current law for circuits when there are no sources or sinks of current in the network. We denote the resistance of the (j,k) bond by $\overline{R}_{jk}$ (and note that $\overline{R}_{kj} = \overline{R}_{jk}$).

With the above notation and Theorem 1 we now conclude that in the multi-saddle case the effective resistance (4.9) is bounded from above by

$$\overline{R} \lesssim \frac{1}{2} \sum_{j \in N} \sum_{k \in N_j} \overline{R}_{jk} I_{jk}^2 \tag{4.22}$$

where the factor $1/2$ is needed because each bond is counted twice. We now minimize (4.22) subject to the condition (4.21) and the discrete analog of the driving condition $< \mathbf{j} >= \mathbf{e}$. If for example $\mathbf{e} = \mathbf{e}_1$, the unit vector in the x direction, we add to the currents I_{jk} satisfying (4.21) a constant current I in the horizontal direction so that the net current crossing any vertical line in Ω equals one while the net current crossing any horizontal line is zero. The equation that the minimizing currents must satisfy is from (4.22)

$$\sum_{j \in N} \sum_{k \in N_j} \overline{R}_{jk} I_{jk} \delta I_{jk} = 0 \tag{4.23}$$

for every current perturbation δI_{jk} that satisfies (4.21) and has no net flow in the horizontal or vertical direction.

The implications of (4.23) are best analyzed by using the dual network which in the case of a rectangular network has the form shown in Fig. 4.1 with broken lines. We denote by $j' \in N'$ the collection of dual nodes and by $N'_{k'}$ the collection of dual nodes adjacent to the dual node k'. The dual network is, of course, the one that is associated with the minima of $\rho^{-1}(\mathbf{x})$, the conductivity of the continuous medium.

A distribution of currents δI_{jk} that satisfies (4.21) and has no net flow in the x or y direction can be written in the form

$$\delta I_{jk} = H_{k'} - H_{j'} \tag{4.24}$$

in terms of a function $H_{j'}$ defined on the dual network. Here (j,k) and (j',k') are related to each other, as is shown in the figure, and the relation

$$\sum_{k \in N_j} \delta I_{jk} = 0$$

is equivalent to

$$\sum_{j \ loop} \Delta H = 0$$

which is the sum of H differences taken over the dual loop surrounding the node j.

We now use (4.24) in (4.23) and note that

$$0 = \sum_{j\in N}\sum_{k\in N_j} \overline{R}_{jk} I_{jk}\delta I_{jk} = \sum_{j'\in N'} (\sum_{k'\in N'_{j'}} (\overline{R}I)_{j'k'}) H_{j'}. \tag{4.25}$$

This basic identity is the analog of integration by parts in the continuum case and says that the sum over nodes of the network can be replaced by a sum over loops of the voltage differences $(\overline{R}I)$ or, what is the same, a sum over the dual nodes. But in (4.25) the $H_{j'}$ are arbitrary since (4.24) must hold for all δI_{jk} subject to (4.21). Thus,

$$\sum_{k'\in N'_{j'}} (\overline{R}I)_{j'k'} = 0,\ j'\in N' \tag{4.26}$$

which is Kirchoff's loop voltage-difference law for circuits. Equation (4.26), the current law (4.21) and the driving condition determine uniquely the minimizing currents I_{jk} in the upper bound (4.22).

To get the asymptotic equality of the effective resistance $\overline{R}$ of the original problem to the upper bound we just described we must show that the lower bound is the same as the upper bound. From Theorem 1 and Lemma 1, we know that we have the bound

$$\overline{R}^{-1} \lesssim \frac{1}{2}\sum_{j'\in N'}\sum_{k'\in N'_{j'}} \overline{R}^{-1}_{j'k'} V^2_{j'k'} \tag{4.27}$$

where $\overline{R}_{j'k'}$ is the resistance associated with the dual bond $(j'k')$ and equals $\overline{R}_{jk}$ from formula (4.4) for the saddle is associated with the bond (jk) in the network or $(j'k')$ in the dual network (see Fig. 4.1). The potential differences $V_{j'k'}$ are defined on the dual network and satisfy the relation $V_{j'k'} = -V_{k'j'}$ as well as

$$\sum_{k'\in N'_{j'}} V_{j'k'} = 0,\ j'\in N' \tag{4.28}$$

which says that the potential differences around a loop (a dual node) vanish. The driving condition in (4.27) is that the net potential difference across any vertical line must equal one (driving in the x direction) while the one across any horizontal line is zero.

With these conditions on $V_{j'k'}$ we can now minimize (4.27) and we find, using the basic identity (4.25) again, Kirchoff's current law for the minimizing potential differences

$$\sum_{k\in N_j} \overline{R}^{-1}_{jk} V_{jk} = 0,\ j\in N. \tag{4.29}$$

But (4.28) and (4.29) are exactly the same equations as (4.21) and (4.26) so, up to scaling by the overall effective resistance, it is clear that the upper bound (4.27) is the same as the reciprocal of the upper bound (4.22) and this proves the asymptotic form of the effective resistance $\overline{R}$ as the one associated with the resistances (4.4) in the network formed from the minima (nodes) of the resistance function $\rho(\mathbf{x})$.

4.3 The Effective Quasistatic Impedance of a High Contrast Continuum. Case A: Series Connection

In this section we consider the problem defined in §3.3 case A. We study the direct problem (2.8) with coefficients $\rho(\mathbf{x}) = \rho_0 e^{-\frac{S(\mathbf{x})}{\epsilon^2}}$ and $C(\mathbf{x}) = C_0 e^{-\frac{P(\mathbf{x})}{\epsilon^2}}$ defined over a region Ω with the geometry shown in Fig. 3.9. The functions $S(\mathbf{x})$ and $P(\mathbf{x})$ are smooth, ρ_0 and C_0 are constants and ϵ is a small parameter. The domain Ω is divided in two regions by a curve L. In region I the resistance dominates ($\rho \gg C$), in region II $C \gg \rho$ and along curve L $\rho = C$. We assume that the resistance $\rho(\mathbf{x})$ has a single saddle $\mathbf{x}_1$ in region I and that the capacitance $C(\mathbf{x})$ has a single saddle $\mathbf{x}_2$ in region II. Both saddles are oriented in the x direction. The current density is divergence free and can be written as $\mathbf{j} = \nabla^{\perp}(u + iv)$, where u and v are the real and imaginary parts of the magnetic field which is perpendicular on the plane Ω. In §3.3 case A we stated that when we have a driving in the x direction (i.e. $< \mathbf{j} >= \mathbf{e}_1$), in the asymptotic limit $\epsilon \to 0$ we have an equivalent series circuit consisting of a resistance $\overline{R}$ placed at the saddle $\mathbf{x}_1$ connected with a capacitance $i\overline{C}$ placed at the saddle $\mathbf{x}_2$. In this section we use the variational principles (2.19) and (2.20) to prove this result.

In the vicinity of the saddle points $\mathbf{x}_1$ and $\mathbf{x}_2$ we have
for $\mathbf{x} \in \delta N(\mathbf{x}_1)$:

$$\begin{aligned} \rho(\mathbf{x}) &\approx \rho(\mathbf{x}_1) exp(-\frac{k_1^-(x-x_1)^2}{2\epsilon^2} + \frac{k_1^+(y-y_1)^2}{2\epsilon^2}) \\ C(\mathbf{x}) &\approx 0, \end{aligned} \tag{4.30}$$

for $\mathbf{x} \in \delta N(\mathbf{x}_2)$:

$$\begin{aligned} \rho(\mathbf{x}) &\approx 0 \\ C(\mathbf{x}) &\approx C(\mathbf{x}_2) exp(\frac{-k_2^-(x-x_2)^2}{2\epsilon^2} + \frac{k_2^+(y-y_2)^2}{2\epsilon^2}). \end{aligned} \tag{4.31}$$

In order to prove the series connection result we have to show that real$(\overline{Z}) = \overline{R}$ and imag$(\overline{Z}) = \overline{C}$. This is done by obtaining matching lower and upper bounds for the effective impedance $\overline{Z}$. For example, in order to obtain an upper bound for real$(\overline{Z})$ we choose some particular real current field $\nabla^{\perp}u$ and then perform the maximization over all the eligible imaginary current fields. From the previous results, we have a good clue for what choice of a real current to make. The current averaged over the whole domain should be $\mathbf{e}_1$, therefore the function $v(x, y)$ is periodic in the domain, whereas the real current can be rewritten with the help of a periodic function $\phi(x, y)$ as $\nabla^{\perp}u = \mathbf{e}_1 + \nabla^{\perp}\phi$. We note that our domain has in the vertical direction the same

boundaries as its component regions I and II and we use the periodicity in y of ϕ and v to show that the currents in the x direction averaged over regions I or II satisfy

$$\begin{aligned}\frac{1}{A_I}\int_I(-u_y)dxdy &= \frac{1}{A_I}\int_I(1-\phi_y)dxdy=1, \quad \frac{1}{A_I}\int_I(-v_y)dxdy=0,\\ \frac{1}{A_{II}}\int_{II}(-u_y)dxdy &= \frac{1}{A_{II}}\int_{II}(1-\phi_y)dxdy=1, \quad \frac{1}{A_{II}}\int_{II}(-v_y)dxdy=0,\end{aligned} \tag{4.32}$$

where A_I and A_{II} are the areas of regions I and II. The currents in the y direction can have different averages as long as they algebraically add to zero. However in this problem both ρ and C have a single saddle point in regions I and II. From the results presented in §3.2 and §5.1 we know that all the current is concentrated around these saddle points. Consider for example $\mathbf{x}_1$, where the function ρ has a minimum in the y direction and a maximum in the x direction. The current will have x component $-u_y$ concentrated around $\mathbf{x}_1$, but the y component u_x should be small. The only place where we could have flow in the y direction would be away from the saddle point, where according to Theorem 1 it should be negligible. The same conclusion applies to region II.

In order to obtain an upper bound on real$(\overline{Z})$, we choose the following real current

$$\nabla^\perp u = \begin{cases} (\frac{1}{\sqrt{\frac{2\pi}{k_1^+}}\epsilon}exp(-\frac{k_1^+(y-y_1)^2}{2\epsilon^2}),0) & \forall \mathbf{x}\in\delta N(\mathbf{x}_1) \\ (\frac{1}{\sqrt{\frac{2\pi}{k_2^+}}\epsilon}exp(-\frac{k_2^+(y-y_2)^2}{2\epsilon^2}),0) & \forall \mathbf{x}\in\delta N(\mathbf{x}_2) \\ \mathbf{0} \quad \text{otherwise} \end{cases} \tag{4.33}$$

which is clearly divergence free, and satisfies

$$<\nabla^\perp u>=<\nabla^\perp u>_I=<\nabla^\perp u>_{II}=\mathbf{e}_1, \tag{4.34}$$

where $<\cdot>$ stands for the normalized average over the indicated region. We use (4.33) in the variational principle (2.19) to obtain

$$\begin{aligned}\text{real}(\overline{Z}) \lesssim \max_{<\nabla^\perp v>=\mathbf{0}} \quad & [\int_{\delta N(\mathbf{x}_1)}\rho(\mathbf{x}_1)e^{-\frac{k_1^-(x-x_1)^2}{2\epsilon^2}+\frac{k_1^+(y-y_1)^2}{2\epsilon^2}}\frac{1}{\frac{2\pi}{k_1^+}\epsilon^2}e^{-\frac{2k_1^+(y-y_1)^2}{2\epsilon^2}}d\mathbf{x}- \\ & 2\int_{\delta N(\mathbf{x}_2)}C\frac{du}{dy}v_y d\mathbf{x} - <\rho(v_x^2+v_y^2)>].\end{aligned} \tag{4.35}$$

We take $\delta N(\mathbf{x}_i)$ to be the squares $\mid x-x_i\mid<\delta$ and $\mid y-y_i\mid<\delta$, $i=1,2$ where the small parameter δ is fixed, so as $\epsilon\to 0$ we have $\frac{\delta}{\epsilon}\to\infty$. The first integral in

(4.35) is

$$\int_{\delta N(\mathbf{x}_1)} \rho(\frac{du}{dy})^2 d\mathbf{x} \approx \frac{\rho(\mathbf{x}_1)}{\frac{2\pi}{k_1^+}\epsilon^2} \int_{|x-x_1|<\delta} e^{-\frac{k_1^-(x-x_1)^2}{2\epsilon^2}} dx \int_{|y-y_1|<\delta} e^{-\frac{k_1^+(y-y_1)^2}{2\epsilon^2}} dy \approx \tag{4.36}$$

$$\rho(\mathbf{x}_1)\sqrt{\frac{k_1^+}{k_1^-}} = \overline{R}.$$

Since the maximum over a sum of functionals is less than the sum of the maxima we have

$$\text{real}(\overline{Z}) \lesssim \overline{R} + \max_{<\nabla^\perp v>=\mathbf{0}}(- < \rho(v_x^2+v_y^2) >) + \max_{<\nabla^\perp v>=\mathbf{0}}(-2\int_{\delta N(\mathbf{x}_2)} C(\mathbf{x})\frac{du}{dy}v_y d\mathbf{x}). \tag{4.37}$$

The trial field $\nabla^\perp u$ is zero in the region $II \setminus \delta N(\mathbf{x}_2)$ so

$$\int_{\delta N(\mathbf{x}_2)} C\frac{du}{dy}v_y d\mathbf{x} = \int_{II} C\frac{du}{dy}v_y d\mathbf{x} = \int_{II}\frac{\partial}{\partial y}[C\frac{du}{dy}v]d\mathbf{x} - \int_{II} v\frac{\partial}{\partial y}[C\frac{du}{dy}]d\mathbf{x}. \tag{4.38}$$

From the periodicity in y of $C\nabla^\perp uv$ and equation $\frac{\partial}{\partial y}(C\frac{du}{dy}) = 0$ satisfied by the trial field (4.33) we obtain that

$$\int_{\delta N(\mathbf{x}_2)} C\frac{du}{dy}v_y d\mathbf{x} \approx 0. \tag{4.39}$$

We should point out that the argument above is not quite right because the real current $\nabla^\perp u$ defined by (4.33) is discontinuous at the boundaries of $\delta N(\mathbf{x}_2)$ so in order to perform the integration by parts in (4.38) we must smooth it out. We introduce the cutoff function

$$\chi_2(y) = \begin{cases} 1 \; for \mid y - y_2 \mid < \delta \\ \\ 0 \; for \mid y - y_2 \mid > \delta + \eta \end{cases}$$

where $\chi_2(y)$ decays smoothly to zero over the region $\delta \leq \mid y - y_2 \mid \leq \delta + \eta$. We modify the trial field $\nabla^\perp u$ in region II to be

$$\nabla^\perp u = \frac{1}{\sqrt{\frac{2\pi}{k_2^+}\epsilon}} e^{-\frac{k_2^+(y-y_2)^2}{2\epsilon^2}} \chi_2(y)\mathbf{e}_1.$$

This is still consistent with $< \nabla^\perp u >_{II} = \mathbf{e}_1$, $\nabla \cdot (\nabla^\perp u) = 0$ and the periodicity in y of the real current. Since v is also periodic in y we obtain from (4.38)

$$\int_{\delta N(\mathbf{x}_2)} C\frac{du}{dy}v_y d\mathbf{x} = -\int_{II} v\frac{\partial}{\partial y}[C\frac{du}{dy}]d\mathbf{x} \approx \tag{4.40}$$

$$\frac{C(\mathbf{x}_2)}{\sqrt{\frac{2\pi}{k_2^+}\epsilon}} \int_{\delta \leq |y-y_2| \leq \delta+\eta} \int_{|x-x_2|\leq\delta} e^{-\frac{k_2^-(x-x_2)^2}{2\epsilon^2}} \frac{d\chi_2}{dy} v(x,y) dx dy.$$

The function $v(\cdot)$ is bounded and after evaluating the Gaussian integral over x we have

$$\int_{\delta N(\mathbf{x}_2)} C\frac{du}{dy}v_y d\mathbf{x} \approx C(\mathbf{x}_2)\sqrt{\frac{k_2^+}{k_2^-}}\int_{\delta\le|y-y_2|\le\delta+\eta} v(x_2,y)\frac{d\chi_2}{dy}dy. \tag{4.41}$$

By assumption $\frac{d\chi_2}{dy}$ is also bounded so from (4.41) we have

$$|\int_{\delta N(\mathbf{x}_2)} C\frac{du}{dy}v_y d\mathbf{x}\ | \ \lesssim K\eta, \tag{4.42}$$

where K is a bounded constant. In conclusion, we can make the integral in (4.42) arbitrary small by choosing η small enough, so inequality (4.37) reduces to

$$\text{real}(\overline{Z}) \lesssim \overline{R} + \max_{<\nabla^\perp v>_I=\mathbf{0}}[-\int_I \rho \mid \nabla^\perp v \mid^2 d\mathbf{x}]. \tag{4.43}$$

The Euler equation for the maximum in (4.43) is

$$\begin{aligned} \nabla^\perp\cdot(\rho\nabla^\perp v) &= 0 \quad \forall\mathbf{x}\in \text{region}I \\ <\nabla^\perp v>_I &= \mathbf{0} \end{aligned} \tag{4.44}$$

and has the solution $\nabla^\perp v = \mathbf{0}$. Thus,

$$\text{real}(\overline{Z}) \lesssim \overline{R}. \tag{4.45}$$

To get a lower bound on real$(\overline{Z})$ we choose in (2.19) the imaginary current $\nabla^\perp v = \mathbf{0}$, and therefore

$$\text{real}(\overline{Z}) \ge \min_{<\nabla^\perp u>=\mathbf{e}_1} <\rho \mid \nabla^\perp u \mid^2> . \tag{4.46}$$

This is exactly the problem studied in §4.1, so we write directly the result given by Theorem 1

$$\text{real}(\overline{Z}) \gtrsim \overline{R}. \tag{4.47}$$

The lower bound on real$(\overline{Z})$ given by (4.47) matches the upper bound (4.45) so real$(\overline{Z}) \approx \overline{R} = \rho(\mathbf{x}_1)\sqrt{\frac{k_1^+}{k_1^-}}$. This result was obtained with a real current, concentrated around the critical points $\mathbf{x}_1, \mathbf{x}_2$ and flowing in the driving direction $\mathbf{e}_1$. The current averaged over our domain, or over regions I, or II is equal to $\mathbf{e}_1$. The analysis for the imag$(\overline{Z})$ is exactly the same, and we obtain

$$\text{imag}(\overline{Z}) \approx \overline{C} = C(\mathbf{x}_2)\sqrt{\frac{k_2^+}{k_2^-}}. \tag{4.48}$$

This completes the analysis of the network approximation for the quasistatic case with one saddle point in the capacitive and resistive region, respectively, in a series configuration.

4.4 The Effective Quasistatic Impedance of a High Contrast Continuum. Case B: Parallel Connection

In this section we consider the problem defined in §3.3 case B. We study the direct problem (2.8) with coefficients $\rho(\mathbf{x}) = \rho_0 e^{-\frac{S(\mathbf{x})}{\epsilon^2}}$ and $C(\mathbf{x}) = C_0 e^{-\frac{P(\mathbf{x})}{\epsilon^2}}$ defined over a region Ω with the geometry shown in Fig. 3.12. The functions $S(\mathbf{x})$ and $P(\mathbf{x})$ are smooth, ρ_0 and C_0 are constants and ϵ is a small parameter. The domain Ω is divided in two regions by a curve L. In region I the resistance dominates ($\rho \gg C$), in region II $C \gg \rho$ and along curve L $\rho = C$. We assume that the resistance $\rho(\mathbf{x})$ has a single saddle $\mathbf{x}_1$ in region I and that the capacitance $C(\mathbf{x})$ has a single saddle $\mathbf{x}_2$ in region II. Both saddles are oriented in the x direction. The current density can be written as $\mathbf{j} = \nabla^{\perp}(u + iv)$, where u and v are the real and imaginary parts of the magnetic field which is perpendicular on the plane Ω. In §3.3 case B we stated that when we have a driving in the x direction (i.e. $< \mathbf{j} >= \mathbf{e}_1$), in the asymptotic limit $\epsilon \to 0$ we have an equivalent parallel circuit consisting of a resistance $\overline{R}$ placed at the saddle $\mathbf{x}_1$ connected with a capacitance $i\overline{C}$ placed at the saddle $\mathbf{x}_2$. In this section we use the variational principles (2.19) and (2.20) to prove this result.

In the vicinity of the saddle points $\mathbf{x}_1$ and $\mathbf{x}_2$ the coefficients $\rho(\mathbf{x})$ and $C(\mathbf{x})$ are given by
for $\mathbf{x} \in \delta N(\mathbf{x}_1)$:

$$\begin{aligned} \rho(\mathbf{x}) &\approx \rho(\mathbf{x}_1) exp(-\frac{k_1^-(x-x_1)^2}{2\epsilon^2} + \frac{k_1^+(y-y_1)^2}{2\epsilon^2}) \\ C(\mathbf{x}) &\approx 0, \end{aligned} \tag{4.49}$$

for $\mathbf{x} \in \delta N(\mathbf{x}_2)$:

$$\begin{aligned} \rho(\mathbf{x}) &\approx 0 \\ C(\mathbf{x}) &\approx C(\mathbf{x}_2) exp(-\frac{k_2^-(x-x_2)^2}{2\epsilon^2} + \frac{k_2^+(y-y_2)^2}{2\epsilon^2}). \end{aligned} \tag{4.50}$$

In order to show the parallel connection we must show that $\overline{Z} \approx (\frac{1}{R} + \frac{1}{i\overline{C}})^{-1}$. This is done by getting matching lower and upper bounds on the effective impedance $\overline{Z}$. In order to obtain an upper bound on real($\overline{Z}$) we choose in the variational principle (2.19) a particular real current $\nabla^{\perp}u$ and then perform the maximization over the imaginary current. The experience gained from studying the static case suggests that the current should be concentrated around the critical points $\mathbf{x}_1$ and $\mathbf{x}_2$. The current averaged over the whole domain should be $\mathbf{e}_1$, and therefore the function v which appears in the expression of the imaginary current must be periodic in Ω. The

real current can be written as $\nabla^\perp u = \mathbf{e}_1 + \nabla^\perp \chi$, where χ is also a periodic function in Ω. We notice that the domain shown in Fig. 3.12 has in the horizontal direction the same boundaries as its component regions I and II. Consequently, the periodicity over x of both χ, and v tells us that the average of the currents in the y direction over each one of the regions will be

$$\begin{aligned} &\frac{1}{A_I}\int_I u_x dxdy = \frac{1}{A_I}\int_I \chi_x dxdy = 0, \quad \frac{1}{A_I}\int_I v_x dxdy = 0, \\ &\frac{1}{A_{II}}\int_{II} v_x dxdy = \frac{1}{A_{II}}\int_{II} \chi_x dxdy = 0, \quad \frac{1}{A_{II}}\int_{II} v_x dxdy = 0 \end{aligned} \tag{4.51}$$

where A_I and A_{II} are the areas of regions I and II. The currents in the x direction can have different averages which must satisfy

$$\begin{aligned} &< -u_y >_I + < -u_y >_{II} = 1 \\ &< -v_y >_I + < -v_y >_{II} = 0. \end{aligned} \tag{4.52}$$

We choose as a real current trial field

$$\nabla^\perp u = \begin{cases} I_1(\frac{1}{\sqrt{\frac{2\pi}{k_1^+}}\epsilon} exp(-\frac{k_1^+(y-y_1)^2}{2\epsilon^2}), 0) & \forall \mathbf{x} \in \delta N(\mathbf{x}_1) \\ I_2(\frac{1}{\sqrt{\frac{2\pi}{k_2^+}}\epsilon} exp(-\frac{k_2^+(y-y_2)^2}{2\epsilon^2}), 0) & \forall \mathbf{x} \in \delta N(\mathbf{x}_2) \\ \mathbf{0} & \text{otherwise} \end{cases} \tag{4.53}$$

which is clearly divergence free. The constants $I_i,\ i = 1, 2$ are the flux of real current through each saddle and according to (4.52) they must satisfy

$$I_1 + I_2 = 1. \tag{4.54}$$

Equation (4.54) is Kirchoff's current law coming from the divergence free condition imposed on the real current. We use (4.53) in the variational principle (2.19) and obtain

$$\begin{aligned} \text{real}(\overline{Z}) \lesssim \min_{I_i} \max_{<\nabla^\perp v>=\mathbf{0}} \quad [\quad &\int_{\delta N(\mathbf{x}_1)} \rho(\mathbf{x}_1) e^{-\frac{k_1^-(x-x_1)^2}{2\epsilon^2} + \frac{k_1^+(y-y_1)^2}{2\epsilon^2}} \frac{I_1^2}{\frac{2\pi}{k_1^+}\epsilon^2} e^{-\frac{2k_1^+(y-y_1)^2}{2\epsilon^2}} d\mathbf{x} - \\ &2 < C\nabla^\perp u \cdot \nabla^\perp v >_{II} - < \rho \mid \nabla^\perp v \mid^2 >]. \end{aligned} \tag{4.55}$$

The neighborhoods of $\mathbf{x}_1$ and $\mathbf{x}_2$ are the squares $\mid x - x_i \mid < \delta,\ \mid y - y_i \mid < \delta,\ i = 1, 2$ where the small parameter δ is fixed, so as $\epsilon \to 0$ we have $\frac{\delta}{\epsilon} \to \infty$. The first term in (4.55) is a Gaussian integral which gives

$$\int_{\delta N(\mathbf{x}_1)} \rho \mid \nabla^\perp u \mid^2 d\mathbf{x} \quad \approx \quad \frac{I_1^2}{\frac{2\pi}{k_1^+}\epsilon^2}\rho(\mathbf{x}_1) \int_{\delta N(\mathbf{x}_1)} exp(-\frac{-k_1^-(x-x_1)^2}{2\epsilon^2} - \frac{k_1^+(y-y_1)^2}{2\epsilon^2}) \approx$$

$$I_1^2\rho(\mathbf{x}_1)\sqrt{\frac{k_1^+}{k_1^-}} = \overline{R}I_1^2. \tag{4.56}$$

From (4.51) and (4.52) we know that the imaginary current in the x direction ($\nabla^\perp v \cdot \mathbf{e}_1 = -v_y$) satisfies

$$< -v_y >_I + < -v_y >_{II} = 0$$

whereas the current in the y direction ($\nabla^\perp v \cdot \mathbf{e}_2 = v_x$) averages to zero in both regions I and II. We introduce the constants J_1 and J_2 which are the fluxes of imaginary current in each region, $< -v_y >_I = J_1$ and $< -v_y >_{II} = J_2$. The average currents must satisfy

$$J_1 + J_2 = 0, \tag{4.57}$$

which is Kirchoff's current law coming from the divergence free condition imposed on $\nabla^\perp v$.

In order to evaluate the integral over $\delta N(\mathbf{x}_2)$ in (4.55) we focus on the current in region II and observe that we can rewrite it as

$$\nabla^\perp v = J_2\mathbf{e_1} + \nabla^\perp \psi \tag{4.58}$$

where ψ is periodic in region II. We also know that $< \nabla^\perp u >= I_2\mathbf{e_1}$ or

$$\nabla^\perp u = I_2\mathbf{e_1} + \nabla^\perp \chi \tag{4.59}$$

where χ is periodic in region II. From (4.58) and (4.59) we have

$$\begin{aligned}\int_{\delta N(\mathbf{x}_2)} C\nabla^\perp u \cdot \nabla^\perp v d\mathbf{x} = J_2 \int_{\delta N(\mathbf{x}_2)} C\nabla^\perp u \cdot \mathbf{e}_1 d\mathbf{x} + \int_{\delta N(\mathbf{x}_2)} C\nabla^\perp u \cdot \nabla^\perp \psi d\mathbf{x} = \\ \frac{J_2}{I_2}\int_{\delta N(\mathbf{x}_2)} C\nabla^\perp u \cdot (I_2\mathbf{e}_1 + \nabla^\perp\chi) d\mathbf{x} + \int_{\delta N(\mathbf{x}_2)} C\nabla^\perp u \cdot \nabla^\perp(\psi - \frac{J_2}{I_2}\chi) d\mathbf{x} = \\ \frac{J_2}{I_2}\int_{\delta N(\mathbf{x}_2)} C \mid \nabla^\perp u \mid^2 d\mathbf{x} + \int_{\delta N(\mathbf{x}_2)} C\nabla^\perp u \cdot \nabla^\perp(\psi - \frac{J_2}{I_2}\chi) d\mathbf{x}.\end{aligned} \tag{4.60}$$

We use the definition (4.53) of the real current and obtain after simple computations

$$\int_{\delta N(\mathbf{x}_2)} C\nabla^\perp u \cdot \nabla^\perp v d\mathbf{x} \approx \frac{J_2}{I_2} C(\mathbf{x}_2)\sqrt{\frac{k_2^+}{k_2^-}} I_2^2 + \int_{\delta N(\mathbf{x}_2)} C\frac{du}{dy}\frac{\partial}{\partial y}(\psi - \frac{J_2}{I_2}\chi) d\mathbf{x}. \tag{4.61}$$

Since $\psi - \frac{J_2}{I_2}\chi$ is periodic in region II, the last integral in (4.61) is similar to (4.39) which was studied in §4.3 and shown to be negligible. We use the notation $\overline{C} = C(\mathbf{x}_2)\sqrt{\frac{k_2^+}{k_2^-}}$ and from (4.55), (4.56) and (4.61) we have

$$\text{real}(\overline{Z}) \lesssim \min_{I_i} \max_{J_i} [\overline{R}I_1^2 - 2\overline{C}I_2J_2 - \min_{<\nabla^\perp v>=J_1\mathbf{e}_1} < \rho \mid \nabla^\perp v \mid^2 >_I]. \tag{4.62}$$

The minimization over region I is similar to the static problem considered in §4.1, therefore

$$\min_{<\nabla^\perp v>=J_1\mathbf{e}_1} < \rho \mid \nabla^\perp v \mid^2 >_I \approx \overline{R} J_1^2. \tag{4.63}$$

Thus, the upper bound on the real part of the effective impedance is

$$\text{real}(\overline{Z}) \lesssim \min_{I_i} \max_{J_i} [\overline{R} I_1^2 - 2\overline{C} I_2 J_2 - \overline{R} J_1^2], \tag{4.64}$$

where the currents I_i and $J_i,\ i = 1, 2$ satisfy Kirchoff's current laws (4.54) and (4.57), respectively.

In order to obtain a lower bound on real$(\overline{Z})$ we choose an imaginary current field

$$\nabla^\perp v = \begin{cases} J_1(\frac{1}{\sqrt{\frac{2\pi}{k_1^+}}\epsilon} exp(-\frac{k_1^+(y-y_1)^2}{2\epsilon^2}), 0) & \forall \mathbf{x} \in \delta N(\mathbf{x}_1) \\ \\ J_2(\frac{1}{\sqrt{\frac{2\pi}{k_2^+}}\epsilon} exp(-\frac{k_2^+(y-y_2)^2}{2\epsilon^2}), 0) & \forall \mathbf{x} \in \delta N(\mathbf{x}_2) \\ \\ \mathbf{0} \quad \text{otherwise} \end{cases} \tag{4.65}$$

which satisfies the divergence free condition and averages to zero ($< \nabla^\perp v >= \mathbf{0}$). We substitute (4.65) in the variational principle (2.19) and after performing similar computations we get a lower bound on real$(\overline{Z})$ which matches the upper bound (4.64). Consequently,

$$\text{real}(\overline{Z}) \approx \min_{I_i} \max_{J_i} [\overline{R} I_1^2 - 2\overline{C} I_2 J_2 - \overline{R} J_1^2]. \tag{4.66}$$

A similar analysis applied to the imaginary part of $\overline{Z}$ (i.e. variational principle (2.20)) leads to the same currents I_i and $J_i,\ i = 1, 2$ and the discrete variational formulation

$$\text{imag}(\overline{Z}) \approx \min_{I_i} \max_{J_i} [\overline{C} I_1^2 + 2\overline{R} I_1 J_1 - \overline{C} J_1^2]. \tag{4.67}$$

The equations that the currents must therefore satisfy are

$$\begin{cases} \overline{R} I_1 \delta I_1 - \overline{C} J_2 \delta I_2 = 0 \\ \\ \overline{C} I_2 \delta J_2 + \overline{R} J_1 \delta J_1 = 0 \end{cases} \tag{4.68}$$

where the perturbation currents δI_i and $\delta J_i,\ i = 1, 2$ are arbitrary but must satisfy Kirchoff's current laws

$$\begin{cases} \delta I_1 + \delta I_2 = 0 \\ \\ \delta J_1 + \delta J_2 = 0. \end{cases} \tag{4.69}$$

From (4.68) and 4.69) we obtain

$$\begin{cases} \overline{R} I_1 = -\overline{C} J_2 \\ \\ \overline{C} I_2 = \overline{R} J_1, \end{cases} \tag{4.70}$$

which are Kirchoff's loop voltage-difference law (discrete version of condition $\nabla \cdot [(\rho + iC)\mathbf{j}] = 0$). From (4.70) and the driving conditions (4.54) and (4.57) we obtain the currents

$$\begin{aligned} I_1 &= \frac{\overline{C}^2}{\overline{R}^2 + \overline{C}^2}, \\ J_1 &= \frac{\overline{RC}}{\overline{R}^2 + \overline{C}^2}, \\ I_2 &= \frac{\overline{R}^2}{\overline{R}^2 + \overline{C}^2}, \\ J_2 &= -\frac{\overline{RC}}{\overline{R}^2 + \overline{C}^2}. \end{aligned} \tag{4.71}$$

Substituting these in the variational principles (4.66) and (4.67) we obtain

$$\overline{Z} \approx (\frac{1}{\overline{R}} + \frac{1}{i\overline{C}})^{-1} \tag{4.72}$$

which is the effective impedance of the parallel network.

This completes the analysis of the network approximation for the quasistatic case with one saddle point in the capacitive and resistive region, respectively, in a parallel configuration.

4.5 High Contrast Approximation in the Quasistatic Case with Many Channels

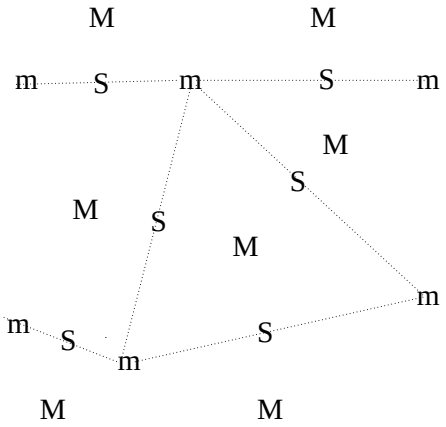

Figure 4.2: Critical points of $\rho(\mathbf{x})$

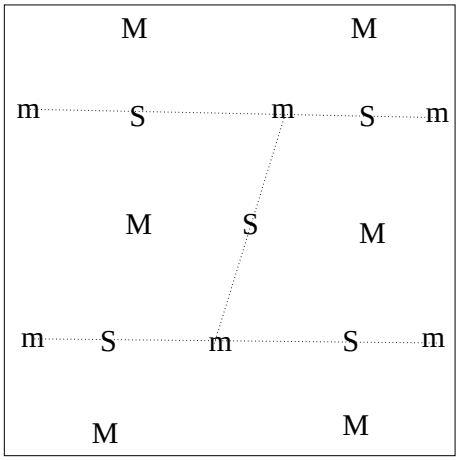

Figure 4.3: Critical points of $C(\mathbf{x})$

The series and parallel resistor-capacitor networks discussed so far are very simple and their connection is evident. In this section we consider more general resistor-capacitor network approximations and show how to connect the resistive and the

capacitive subnetworks in the domain. We recall that periodicity of the boundary value problem is not necessary for the applicability of the network approximation. We have used periodicity throughout the paper to simplify the analysis, which is valid for general, nonperiodic structures and arbitrary boundary conditions.

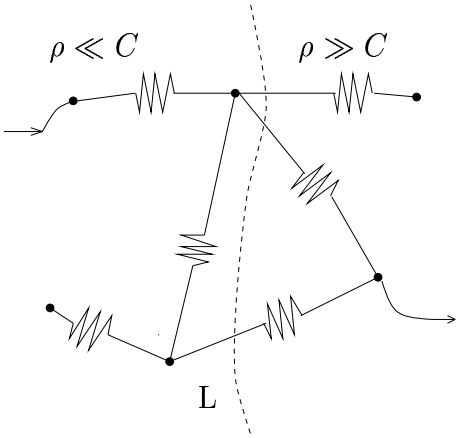

Figure 4.4: Resistor network

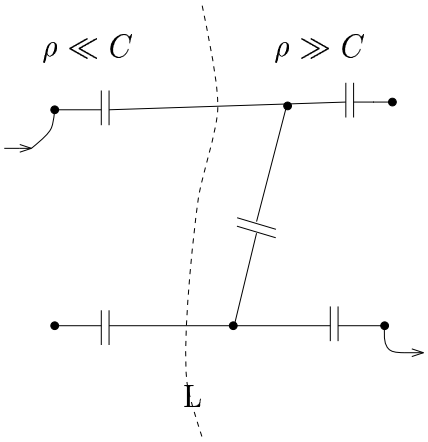

Figure 4.5: Capacitor network

We explain the way the networks are connected by considering a high contrast medium with one region with dominant resistance separated from a region with dominant capacitance by an interface L along which ρ equals C. The current flow may arise from any kind of boundary conditions; the results of this section hold in general. To fix ideas we assume that we have a point current source along the left boundary and a point current sink along the right boundary, as shown in Figs 4.4,4.5. Everywhere else we impose homogeneous Neumann boundary conditions.

We assume that $\rho(\mathbf{x})$ and $C(\mathbf{x})$ have the critical points (maxima, minima and saddles) shown in figures 4.2 and 4.3 with symbols M, m, and S, respectively. Consider first the resistive and capacitive structures separately, ignoring the interface L that identifies the dominant one. Transport in a high contrast material with resistance ρ that has critical points as shown in Fig. 4.2 is approximated by that of a resistor network with nodes at the minima of ρ and branches passing through the saddle points of ρ (see Fig. 4.4). The connection of the current source and sink to the network dependents on their position relative to the basins of attraction of the minima of the resistance (nodes in the network) that are closest to the boundary. For the example we are considering the connection is shown in Fig. 4.4. The capacitor network approximation is obtained in a similar way and is shown in Fig. 4.5.

Now we return to the full quasistatic resistive-capacitive medium and cut the approximating resistor and capacitor networks with the dividing interface L, as shown in figures 4.4 and 4.5. Note that since the flow concentrates only at saddle points of ρ or C (resistors or capacitors in the approximating circuit) and merges in the vicinity of the minima of ρ or C (nodes in the network), if there is any flow concentration across the interface L then the region around it must be in the basin of attraction of

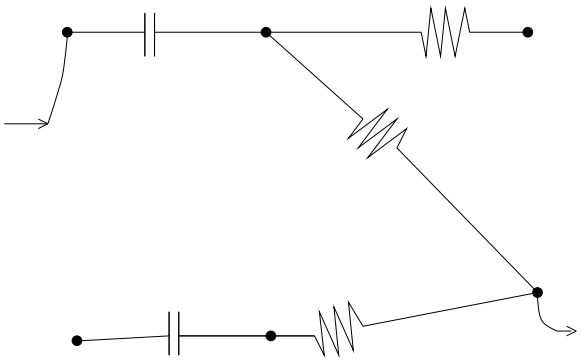

Figure 4.6: Equivalent resistor-capacitor network

a node (minimum) in the resistor network and a node (minimum) in the capacitor network. Thus, both ρ and C must have a minimum along the interface L, in that region. However, ρ equals C along L so the nodes in the resistive and capacitive networks that have the minimum on L within their basin of attraction are connected to each other. This means that we cannot have an arbitrary arrangement of resistive and capacitive nodes on opposite sides of the interface L; they must be configured compatibly.

The high-contrast resistor-capacitor network is, therefore, determined as follows. We cut the resistor and capacitor networks along L, as shown in Fig. 4.4 and 4.5, and identify regions of flow-merging (around minima of ρ and C) on either side of it. We also identify the resistive and capacitive nodes (minima) that correspond to them and connect the loose branches in the resistive region that end in the resistive nodes with the loose branches in the capacitive region that end in the adjacent capacitive nodes. The connection for the example considered is shown in Fig. 4.6.

The construction of the resistor-capacitor network for high contrast media generalizes to an arbitrary number of regions with dominant resistive and capacitive properties. However, special, nongeneric configurations need additional considerations. For example, when critical points of ρ and C are on the dividing interface L, a special situation, a more detailed analysis is needed.

5 Numerical Computations

We now present the results of some numerical experiments that illustrate the analysis carried out in this paper. We use a Fourier-Galerkin spectral method to solve equation (2.10) with periodic boundary conditions in a square domain $\Omega = [0, 2\pi] \times [0, 2\pi]$. We compute the effective impedance as given by equation (2.14). The domain Ω is uniformly discretized with a square mesh of side $h = 2\pi/64$ and the integral in (2.14)

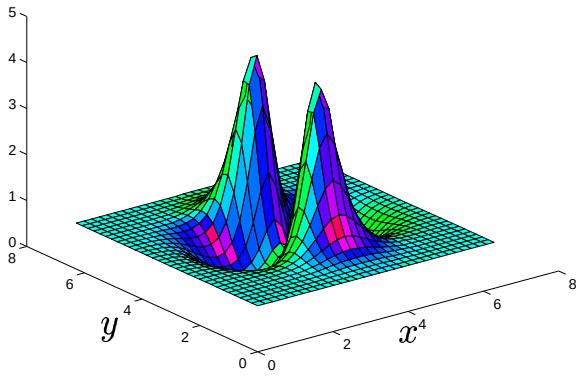

Figure 4.7: Example of a function $\rho(\mathbf{x})$ that has a saddle point in the domain

is computed with Simpson's rule.

5.1 Static Fields and Resistive Circuits

We first test the high contrast approximation for transport through a conducting medium. The approximation articulates the flow channeling that occurs around saddle points of the high contrast conductance or resistance. We consider media that have a single saddle point of the resistance ρ in the domain so the approximating networks consist of a single resistor, given by (3.15)).

The resistance function $\rho(\mathbf{x})$ that we use has the simple geometry of §3.2, Fig. 3.7. The saddle point of ρ is located at $\mathbf{x}_S = (\pi, \pi)$, the minima are at $\mathbf{x}_{m1} = (\pi, 2.432)$ and $\mathbf{x}_{m2} = (\pi, 4.054)$ and the maxima at $\mathbf{x}_{M1} = (2.432, \pi)$ and $\mathbf{x}_{M2} = (4.054, \pi)$, respectively. The value of the resistance in the channel $\rho(\mathbf{x}_S)$, the curvatures k^+, k^- and the parameter ϵ vary for different numerical experiments (see section §3.2 for the definition of these parameters). To test the effective resistance formula $\overline{R} \approx \rho(\mathbf{x}_S)\sqrt{\frac{k^+}{k^-}}$, discussed in §3.2, we fix the parameter $\epsilon^2 = 0.06$ and vary the height of the saddle $\rho(\mathbf{x}_S)$ and the curvature parameters k^+, k^-. The results reported in table 5.1 show that the approximation is accurate to within 5% for the lower contrast experiments and 2% for the high contrast of 209.2.

The accuracy of the resistor approximation is expected to depend on the contrast $\max(\rho)/\min(\rho)$, so we test it further by fixing the curvatures $k^+ = 2.4$ and $k^- = 1.6$ and varying ϵ. The results reported in table 5.2 show that for contrast of order (10^2) the error is small but the approximation is quite inaccurate for lower contrasts. As we show in Fig. 4.8, for a sufficiently high contrast of the flow is channeled at the saddle point of ρ and the asymptotic analysis holds. However, when the contrast is low (see Fig. 4.9), the current flow is spread out throughout the domain and the

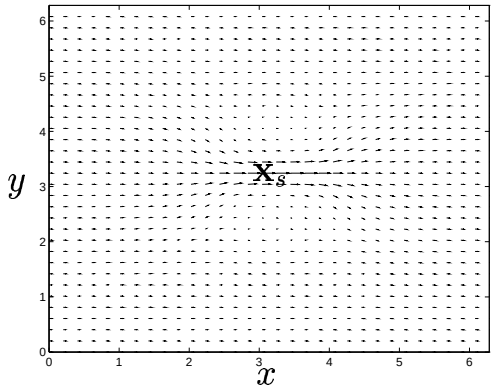

Figure 4.8: Flow concentrated at the saddle point of the resistance for a contrast $\max(\rho)/\min(\rho) = 209.2$

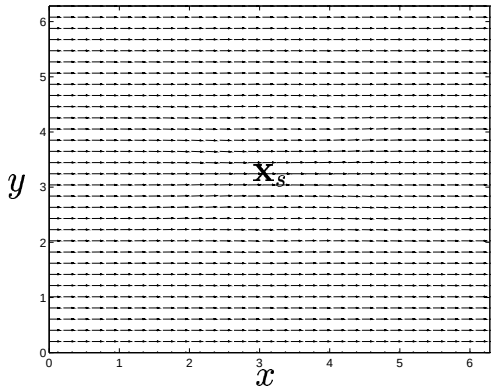

Figure 4.9: Flow is spread out and not concentrated at the saddle point of the resistance for a contrast of ρ lowered to 9.1

$\rho(\mathbf{x}_s)$	k^+	k^-	Contrast	$\overline{R}$	$\overline{R}_{num}$	Rel. error (%)
1.	1.4	1.8	70.1	1.1339	1.2011	5.39
4.1727	2.6	3.4	89.3	3.6489	3.4714	-4.86
2.0427	0.8	2.	97.1	1.2919	1.3478	4.33
4.1727	2.4	1.6	209.2	5.1105	5.2114	1.97

Table 5.1: Dependence of $\overline{R}$ on the resistance and curvatures at the saddle point

resistor approximation is inaccurate.

5.2 Quasistatic Fields and Resistor-Capacitor Circuits

We now test the high contrast approximation by discrete resistor-capacitor networks for quasistatic flows.

Case A: Series connection

To test the range of validity of the resistor-capacitor series network approximation we consider functions $\rho(\mathbf{x})$ and $C(\mathbf{x})$ with geometry similar to the one in §3.3 Case A. In Fig. 5.1 and 5.2 we show an example of functions $\rho(\mathbf{x})$ and $C(\mathbf{x})$ used in this section. The resistive and capacitive regions are separated by the interface at $x = \pi$ along which $\rho = C$. The location of the saddle points, the curvatures of the scaled logarithms of ρ and C at the saddles and the contrast are varied different numerical experiments. As discussed in §3.3 Case A, we can have, in addition to the saddle points, regions of *weak* flow concentration that are negligible in the computation of

Contrast	$\rho(\mathbf{x}_s)$	ϵ^2	$\overline{R}$	$\overline{R}_{num}$	Rel. error (%)
9.1	1.1331	0.8	1.3878	1.1744	15.38
52.6	1.1814	0.6	1.4469	1.3281	-8.21
65.3	1.3956	0.3	1.7093	1.8176	6.34
165	2.7183	0.1	3.3292	3.4212	2.46
209.2	4.1727	0.06	5.1105	5.2114	1.97

Table 5.2: Accuracy of the resistor network approximation versus the contrast

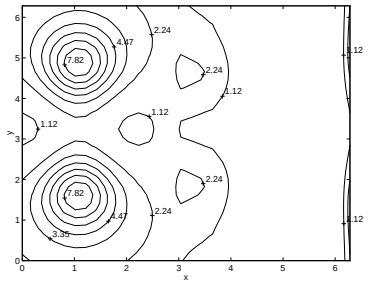

Figure 5.1: Microscopic resistance $\rho(\mathbf{x})$

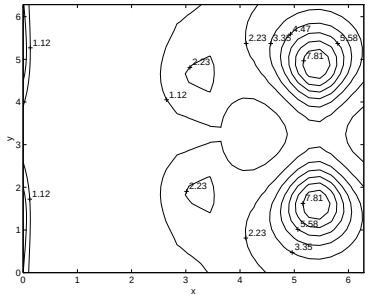

Figure 5.2: Microscopic capacitance $C(\mathbf{x})$

the effective impedance in the limit of infinitely high contrast. An example of such a region is the common minimum $\xi = (\pi, \pi)$ of ρ and C along the dividing interface at $x = \pi$.

In order to test the accuracy of the resistor-capacitor series network approximation for different contrasts we fix the curvature parameters (see (3.18) and (3.19)) $k_1^+ = k_1^- = k_2^+ = 1.$, $k_2^- = 1.6$ and the location of the saddle points $\mathbf{x}_1 = (\pi/3, \pi)$ and $\mathbf{x}_2 = (5\pi/3, \pi)$, respectively. The contrast of ρ and C is changed by varying the parameter ϵ. The results of this set of experiments are reported in table 5.3. As expected, the approximation is accurate to within a few percent when the contrast is $O(10^2)$ or higher and quite inaccurate for lower contrasts. The flow corresponding to the first entry in table 5.3 is shown in Fig. 5.3. We only show the real part of the current flow. The imaginary part is four orders of magnitude smaller than the real part, as predicted by the asymptotic theory in §3.2 Case A. We note the strong flow concentration around the saddle points of ρ and C and the concentration at the minimum ξ along the interface separating the resistive from the capacitive region. However, around ξ the magnitude of the current increases only along the y direction. Across the interface (x direction), the potential gradient is negligible so we only have weak flow concentration at ξ. Thus, in the circuit approximation, the contribution of this region is equivalent to having a connecting wire of negligible impedance.

The resistor-capacitor series network approximation was also tested for different

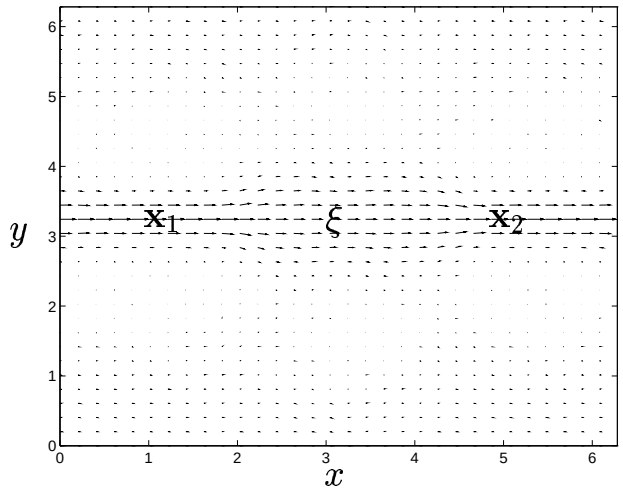

Figure 5.3: Real current flow for a contrast of ρ and C of 1015.7

$\rho(\mathbf{x}_1)$	$C(\mathbf{x}_2)$	Contrast	ϵ^2	$\overline{R}$	$\overline{R}_{num}$	Rel. Error	$\overline{C}$	$\overline{C}_{num}$	Rel. Error
28.0316	28.0316	1015.7	0.06	28.0316	29.0506	3.64 %	22.1609	22.2818	0.6 %
17.4117	17.4117	978.4	0.07	17.4117	18.0364	3.59	13.7652	13.8814	0.84
12.1825	12.1825	853.7	0.08	12.1825	12.6136	3.54	9.631	9.8037	1.73
5.2945	5.2945	113.4	0.12	5.2945	5.0600	-4.43	4.1857	4.0979	-2.10
2.7183	2.7183	37.9	0.2	2.7183	2.3028	-15.	2.1490	1.9925	-7.28
1.9477	1.9477	9.45	0.3	1.9477	1.5001	-23.	1.5398	1.3472	-12.5

Table 5.3: Accuracy of the R-C series network approximation versus the contrast

locations and orientations of the saddle points in the resistive and capacitive regions. The results are not influenced much, as expected, because location and orientation of the saddles does not affect the network.

Case B: Parallel connection

In the quasistatic regime we now explore the high contrast approximation with a parallel resistor-capacitor networks. The geometry of the microscopic resistance and capacitance is similar to the one in §3.3 Case B. In Fig. 5.4 and 5.5 we show an example of functions $\rho(\mathbf{x})$ and $C(\mathbf{x})$ used in this section. The resistive and capacitive regions are separated by the interface $y = \pi$ along which ρ and C have a common minimum at $\xi = (\pi, \pi)$.

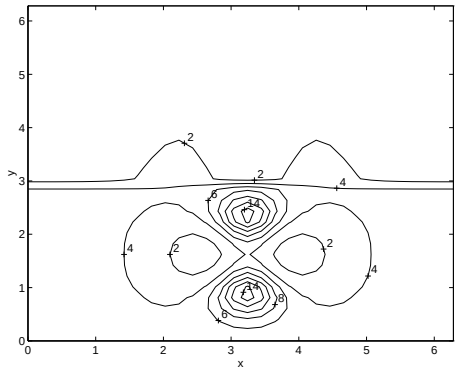

Figure 5.4: Microscopic resistance $\rho(\mathbf{x})$

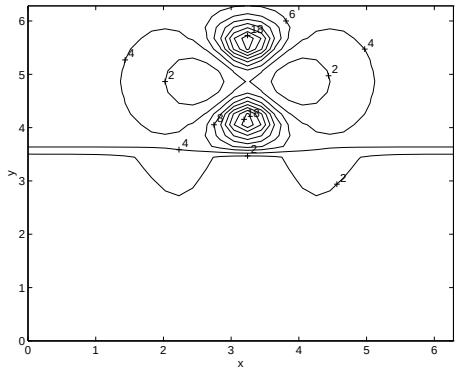

Figure 5.5: Microscopic capacitance $C(\mathbf{x})$

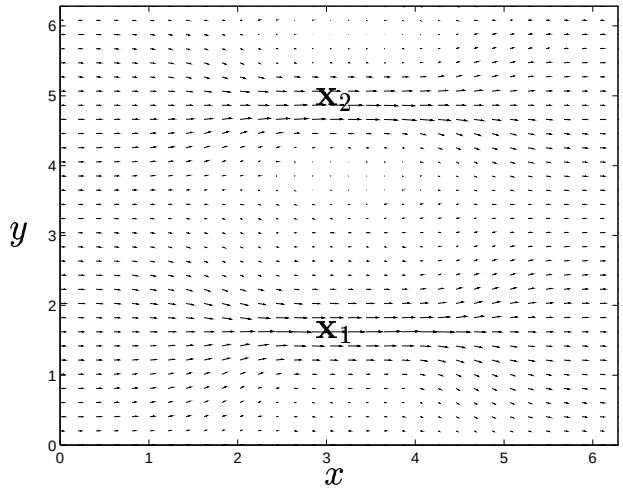

Figure 5.6: Real current flow for a contrast of ρ and C of 853.7

We test the accuracy of the network approximation for different contrasts of ρ and C in a set of experiments with the location of the saddle points kept at $\mathbf{x}_1 = (\pi, \pi/3)$ and $\mathbf{x}_2 = (\pi, 5\pi/3)$ and with the curvature parameters fixed at $k_1^+ = k_1^- = k_2^- = 1.$ and $k_2^+ = 1.6$. The contrast is varied by changing the parameter ϵ.

In tables 5.4 and 5.5 we show the error in the effective impedance and the theoretical and numerically computed current fluxes through the channels at the saddle points of ρ and C ($\alpha_i,\ \beta_i,\ i = 1, 2$ are defined in §3.3 case B). The results show that the parallel resistor-capacitor network approximation is accurate to within few percent when the contrast of ρ and C is $O(10^2)$ or higher. For lower contrasts, the approximation is not inaccurate. The real part of the current flow computed with contrast of ρ and C equal to 853.7 is shown in Fig. 5.6 . The imaginary part of the current behaves similarly except that while in the resistive channel the flow is in the

$\rho(\mathbf{x}_1)$	$C(\mathbf{x}_2)$	ϵ^2	real$(\overline{Z})$	real $(\overline{Z}_{num})$	Rel. Error	imag$(\overline{Z})$	imag $(\overline{Z}_{num})$	Rel. Error
12.1825	12.1825	0.08	7.4961	7.3967	-0.82 %	5.9256	5.8333	-1.56 %
7.3891	7.3891	0.1	4.5471	4.1970	-7.7	3.6955	4.1172	11.41
3.7937	3.7937	0.15	2.3346	1.8712	-19.85	1.8457	1.1394	-27.43
2.7183	2.7183	0.2	1.6728	0.8918	-46.7	1.3225	0.8442	-36.17

Table 5.4: Accuracy of the R-C parallel network for different contrasts of ρ and C

Contrast	α_1	α_1^{num}	β_1	β_1^{num}	α_2	α_2^{num}	β_2	β_2^{num}
853.7	0.6154	0.6120	0.4865	0.4783	0.3846	0.3880	-0.4865	-0.4783
140.8	0.6154	0.6013	0.4865	0.4592	0.3846	0.3987	-0.4865	- 0.4592
89.4	0.6154	0.5534	0.4865	0.3621	0.3846	0.4466	-0.4865	-0.3621
37.9	0.6154	0.509	0.4865	0.2132	0.3846	0.4910	-0.4865	-0.2132

Table 5.5: Real and imaginary current fluxes through the channels developed at the saddle points of ρ and C

positive direction of the x axis, in the capacitive channel the flow is in the opposite direction. This behavior is, of course, due to the zero imaginary part of the driving condition assumed in the computations. The behavior of the current flow confirms the results of the asymptotic theory that is, that the flow concentrates only in the channels that form at saddle points of the microscopic resistance and capacitance.

6 Summary and Conclusions

We have shown both analytically and numerically that the effective resistance and capacitance of a high contrast material can in certain cases be approximated well by a resistor-capacitor (R-C) network. In both the static case, where the network consists only of resistors, as well as in the quasistatic case, this can be done in general for any number of saddle points of the resistance and capacitance functions $\rho(\mathbf{x})$, $C(\mathbf{x})$, around which the current concentrates. Variational principles play an essential role in the analysis. We have restricted attention to two dimensional problems but the results are general and extend easily to any number of dimensions.

Network approximations do not seem to be appropriate for quasistatic resistive-inductive problems because we do not have flow concentration around saddles. There are variational principles for these problems but we do not know how to use them yet.

In [10] we have used the local analysis of the flow around the saddles to construct

a very efficient and accurate hybrid, analytical-numerical method for solving high contrast conductivity problems. In [8] we have used the static asymptotic theory to image high contrast media with impedance tomography.

Acknowledgements

This work was partially supported by a grant from AFOSR, F49620-94-1-0436 and by the NSF, DMS 9308471. We thank J. Berryman for many fruitful discussions and advice on this problem.

References

[1] Alumbaugh, D. L., 1993, *Iterative Electromagnetic Born Inversion Applied to Earth Conductivity Imaging*, Ph.D. thesis, Berkeley.

[2] Alumbaugh, D.L., Morrison, H. F., 1993, *Electromagnetic conductivity imaging with an iterative Born inversion*, IEEE Transactions on Geosciences and Remote Sensing, Vol. 31, No. 4, pp. 758-763.

[3] Ambegaokar, V., Halperin, B. I., Langer, J. S., 1971, *Hopping Conductivity in Disordered Systems*, Phys. Rev. B, 4(8), pp 2612-2620.

[4] Batchelor, G. K., O'Brien, R. W., 1977, *Thermal or electrical conduction through a granular material*, Proc. R. Soc. London A, 355, pp 313-333.

[5] Bensoussan, A., Lions, J. L., Papanicolaou, G. C., 1978, *Asymptotic analysis for periodic structures*, North-Holland, Amsterdam.

[6] Berlyand, L., Golden, K., 1994, *Exact result for the effective conductivity of a continuum percolation model*, Physical Review B (Condensed Matter), vol.50, no.4, pp 2114-17.

[7] Borcea, L., 1996, *Direct and Inverse Problems for Transport in High Contrast Media*, Ph.D. thesis, Stanford University.

[8] Borcea, L., Berryman, J. G., Papanicolaou, G. C., 1996, *High Contrast Impedance Tomography*, Inverse Problems, 12, pp 1-24.

[9] Borcea, L., Papanicolaou, G. C, Wehr, J., *Network approximation for high contrast random conductivities*, in preparation.

[10] Borcea, L., Papanicolaou G. C., *A Hybrid Numerical Method for High Contrast Conductivity Problems*, to appear in J. Computational and Applied Mathematics, 1996.

[11] Cherkaev, A. V., Gibiansky, L. V., 1994, *Variational principles for complex conductivity, viscoelasticity, and similar problems in media with complex moduli*, J. Math. Phys., 35 (1), pp 127-145.

[12] Clerc, J.P., Giraud, G., Laugier, J.M. and Luck, J.M., 1990, *The electrical conductivity of binary disordered systems, percolation clusters, fractals and related models*, Advances in Physics, 39 (3), pp 191-309.

[13] Dagan, G., 1989, *Flow and Transport in Porous Formations*, Springer- Verlag, New York.

[14] Dykhne, A. M., 1971,*Conductivity of a two-dimensional two-phase system*, JETP 32, pp 63-65.

[15] Ekeland, I., Teman, R., 1976, *Convex analysis and variational problems*, Studies in mathematics and its applications, vol. 1.

[16] Fannjiang, A., Papanicolaou, G., 1994, *Convection enhanced diffusion for periodic flows*, SIAM J. Appl. Math., 54, pp 333-408.

[17] Fannjiang, A., Papanicolaou, G., 1996, *Diffusion in turbulence*, Probability Theory and Related Fields, 105, pp 279-334.

[18] Fannjiang, A., Papanicolaou, G.C., 1996,*Convection enhanced diffusion for random flows*, to appear in the Journal of Statistical Physics.

[19] Gibiansky, L. V., Milton, G. W., 1993, *On the effective viscoelastic moduli of two-phase media. Rigorous bounds on the complex bulk modulus*, Proc. R. Soc. London A, 440, pp 163-188.

[20] Golden, K.M., *Percolation models for porous media*, in Homogenization and Porous Media, U. Hornung, ed., Springer Verlag, in press.

[21] Golden, K.M., Kozlov, S.M., *Critical path analysis of transport in highly disordered random media*, preprint 1995.

[22] Golden, K., Papanicolaou, G., 1985, *Bounds for effective parameters of multicomponent media by analytic continuation*, J. Stat. Phys. 40, pp 655-668.

[23] Habashy, T. M., Groom, R. W., Spies, B. R., 1993, *Beyond the Born and Rytov Approximations: A nonlinear approach to Electromagnetic Scattering*, Geophysical Research, Vol. 98, No. B2, pp 1759-1755, February.

[24] Halperin, B. I., 1989, *Remarks on percolation and transport in networks with a wide range of bond strengths*, Physica D, 38, pp 179-183.

[25] Hashin, Z., Shtrikman, S., 1962, *A variational approach to the theory of the effective magnetic permeability of multiphase materials*, J. Appl. Phys. 33, pp 3125-3131.

[26] Jackson, J. D., 1974, *Classical Electrodynamics*, second ed., Wiley, New York.

[27] Jikov, V. V., Kozlov, S. M., Oleinik, O. A., 1994, *Homogenization of Differential Operators and Integral Functional*, Springer-Verlag, Berlin Heilderberg.

[28] Keller, J. B., 1963, *Conductivity of a Medium Containing a Dense Array of Perfectly Conducting Spheres or Cylinders or Nonconducting Cylinders*, J. Appl. Phys., 34 (4), pp 991-993.

[29] Keller, J. B., 1987, *Effective conductivity of periodic composites composed of two very unequal conductors*, J. Math. Phys., 28 (10), pp 2516-2520.

[30] Keller, J. B., 1964, *A Theorem on the Conductivity of a Composite Medium*, J. Math. Phys., 5(4), pp 548-549.

[31] Kitanidis, P. K., 1995, *Quasilinear Geostatistical Theory for Inversing*, Water Resour. Res., 31, pp 2411-2419.

[32] Kohler, W., Papanicolaou, G., 1982, *Bounds for the effective conductivity of random media*, Springer Lecture Notes in Physics 154, pp 111-130.

[33] Koplik, J., 1982, *Creeping flow in two-dimensional networks*, J. Fluid Mech., Vol. 119, pp 219-247.

[34] Kozlov, S. M., 1989*Geometric aspects of averaging*, Russian Math. Surveys 44:2, pp 91-144.

[35] Milton, G. W., 1990, *On characterizing the set of possible effective tensors of composites: The variational method and the translation method*, Communications on Pure and Applied Math., Vol XLIII, pp 63-125

[36] Schwartz, L. M., Banavar, J. R., Halperin, B. I., 1989, *Biased-diffusion calculations of electrical transport in inhomogeneous continuum systems*, Physical review B, Vol. 40, 13, pp 9155-9161.

[37] Shah, C. B., Yortsos, Y. C., 1996, *The permeability of strongly-disordered systems*, Physics of Fluids, vol.8, no. 1, pp 280-282.